# SYNTHESIS AND CHARACTERIZATION OF FERROMAGNETIC NANOWIRES

by

POCHING TSAI

Presented to the Faculty of the Graduate School of

The University of Texas at Arlington in Partial Fulfillment

of the Requirements

for the Degree of

MASTER OF SCIENCE IN MATERIALS SCIENCE AND ENGINEERING

THE UNIVERSITY OF TEXAS AT ARLINGTON

August 2010

ACKNOWLEDGEMENTS

I would like to express my sincere gratitude to my advisor, Professor J. Ping Liu, for providing invaluable guidance to research and constant supports to my study. I highly appreciate Prof. Liu for introducing me to scientific research, giving me a chance to accelerate my research skills, and encouraging me to work in the field of nanotechnology. His expertise in nanostructured magnetic materials along with his vision on nanotechnology has been the source of inspiration to me for further research in the field. The present research work would, therefore, have never been completed without his proper guidance, regular supervision, and constant encouragement.

I would like to thank Professors Wen S. Chan and Michael Jin for serving on my thesis supervisory committee. I am grateful to them for their careful and critical reading of my thesis and invaluable suggestions. Their comments and suggestions would not only help to improve my research skill but also would be a great help to have a deeper insight into the future research.

I would also like to thank Prof. Chuanbin Rong, Dr. Narayan Poudyal, Dr. Girija Shankar Chaubey, Dr. Yajing Zhang, Dr. Nguyen Van Vuong, Dr. Shirly Machluf for their invaluable suggestions, guidance, and encouragement. Their technical support with equipments was a great help. I am thankful to Prof. Chuanbin Rong, Dr. Narayan Poudyal who have reviewed my thesis.

I am thankful to our collaborator, Dr. Z.L. Wang in Georgia Institute of Technology for his cooperation in HRTEM analysis. I am thankful to Dr Jiechao Jiang for the technical support in operating the Transmission Electron Microscope and the assistance in processing TEM images.

I would like to thank my colleagues, DaPeng Wang, Vikas Nandwana, Hamed Arami for their cooperation in the laboratory activities. I express my indebtedness to these friends for their encouragement to complete this work. There can be no adequate acknowledgement for the loving encouragement I have received from my parents, brother and sister and all family members. Without their constant support and inspirations all this would never have been possible. This work was supported by US DoD/MURI grant N00014-05-1-0497 and DARPA through ARO under Grant No DAAD 19-03-1-0038.

August 2, 2010

ABSTRACT

SYNTHESIS AND CHARACTERIZATION OF FERROMAGNETIC NANOWIRES

PoChing Tsai, M.S.

The University of Texas at Arlington, 2010

Supervising Professor: J.Ping Liu

Ferromagnetic nanocrystals with shape anisotropy have drawn great attention in the past decades because of their unique magnetic properties and for their potential applications in ultra-high-density magnetic recording media, exchange-coupled nanocomposite magnets and related nanodevices. In this thesis, synthesis and characterixation of ferromagnetic CoNi and CoFe nanowires are reported.

CoNi nanocrystals with different size, shape and composition were successfully synthesized via a catalyst chemical solution method. It was found out that the structure and morphology can be controlled by altering the NaOH concentration, and the

elongation of the nanowires can be adjusted by changing surfactants ratio and catalyst amount.

Unlike the CoNi, CoFe nanocrystals were prepared by a non-catalyst chemistry solution method. The particle size and shape are controlled by varying parameters such as solvent amount, surfactant ratio, reducing agent and heating rate.

Morphological, structural, and compositional characterizations of the nanoparticles were performed by using Transmission Electron Microscopy (TEM), high resolution TEM (HRTEM), and X-Ray Diffractometer (XRD). Magnetic properties of nanoparticles of different size were studied by Alternating Gradiant Magnetometer (AGM).

TABLE OF CONTENTS

LIST OF ILLUSTRATIONS

Figure Page

# CHAPTER 1

# MAGNETISM AND MAGNETIC MATERIALS

## 1.1. Basics of Magnetism

### *1.1.1 Origin of Magnetism*

Magnetism is a physical phenomenon of attractive or repellent forces between materials, and these forces are related to magnetic fields which are generated by a magnet or an electric current. An electromagnet is a type of magnet whose magnetic field is generated by a flow of electric current. On the other hand, a permanent magnet is a type of magnets made from the materials which are magnetized and produces a magnetic field. The electromagnetic field will disappear when electric current is removed, but a permanent magnet keeps its magnetism for a long time. For a permanent magnet, it is known that fundamental magnetic units are the extranuclear electrons. These electrons are moving around a nuclear and create an orbital magnetic moment (Figure 1.1). There is also a magnetic moment assumed to be associated with an electron spinning motion, called spin magnetic moment. Most of elements have no magnetic moment due to reason that the moments of pair electrons are cancelled each other, but a few elements (Iron, Cobalt and Nickel) with unpaired spins have net magnetic moment.[1-2]

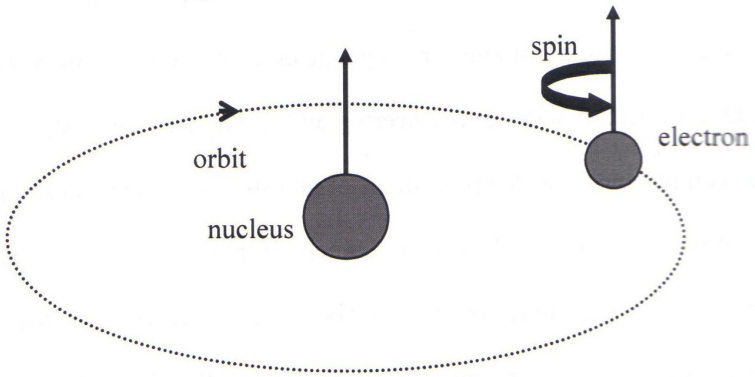


Figure 1.1 Orbit of a spinning electron about the nucleus of an atom

*1.1.2 Magnetic Field and Magnetic Moment*

When a magnetic field **H** is applied on a material, the response of the material is called magnetic induction or magnetic flux density **B**, and the relationship between **H** and **B** is a property of material, called the intensity of magnetization **M**. The equation relating **H**, **B** and **M** is (in cgs units)

$$\mathbf{B} = \mathbf{H} + 4\pi \mathrm{M} \tag{1.1}$$

The magnetization M is defined as the magnetic moment per unit volume.

$$\mathbf{M} = \mathbf{m} / \mathbf{V} \ (\mathrm{emu/cm^3}) \tag{1.2}$$

The properties of a material are defined by the way in which these quantities vary with the applied magnetic field. The ratio of M to H is called susceptibility $\chi$.

$$\chi = \mathrm{M} / \mathrm{H} \ (\mathrm{emu/cm^3 Oe}) \tag{1.3}$$

The ratio which indicates how permeable the material is to the magnetic field is called permeability, $\mu$.

$$\mu = B / H \text{ (gauss/Oe)} \qquad (1.4)$$

By observing the susceptibility and permeability of material, different type of magnetism can be characterized.

## 1.2. Classification of Magnetism

Materials can be classified by the response to an external magnetic field applied to them. The $\chi$ value of materials is changed with different magnetic field intensity and temperature. The magnetic behavior of materials can be divided into diamagnetism, paramagnetism, ferromagnetism, anti-ferromagnetism and ferrimagnetism. Figure 1.2 shows types of magnetism of all elements.

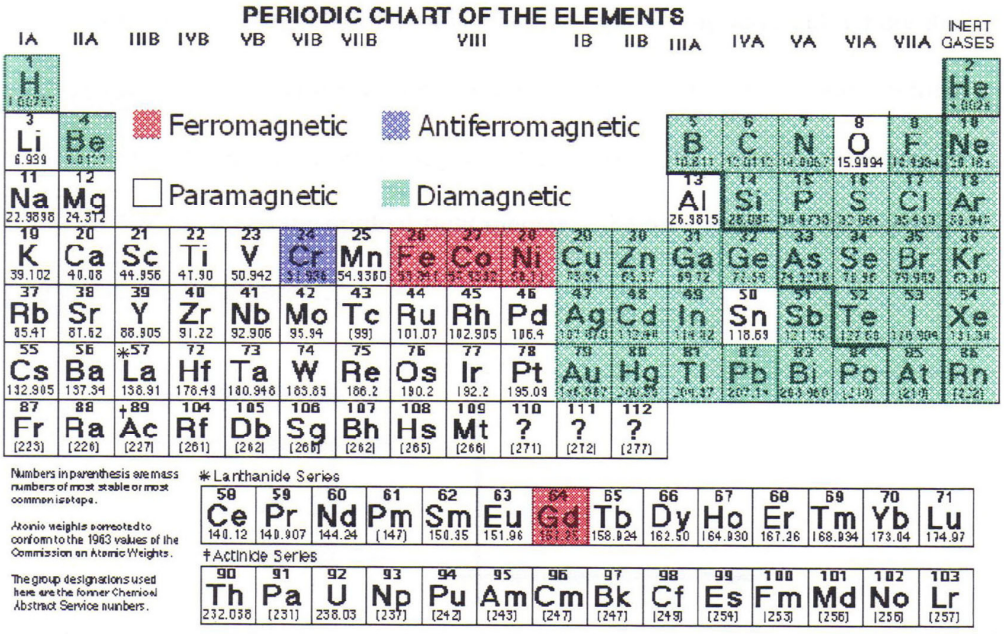


Figure 1.2 A periodic table shows the types of magnetic behavior of the elements at room temperature.

*1.2.1 Diamagnetism*

Diamagnetism is a very week magnetism that happened in all materials. To explain this phenomenon, consider the electrons which are moving on the orbital as a current-carry coil. If it is applied in a magnetic field, it will generate another current in opposite direction. The magnetic moment induced by this new current will against to the external field. Finally, a negative magnetization is occurred, and the susceptibility $\chi$ is less than 0, temperature independent and of the order of $10^{-5}$. (Figure 1.3).

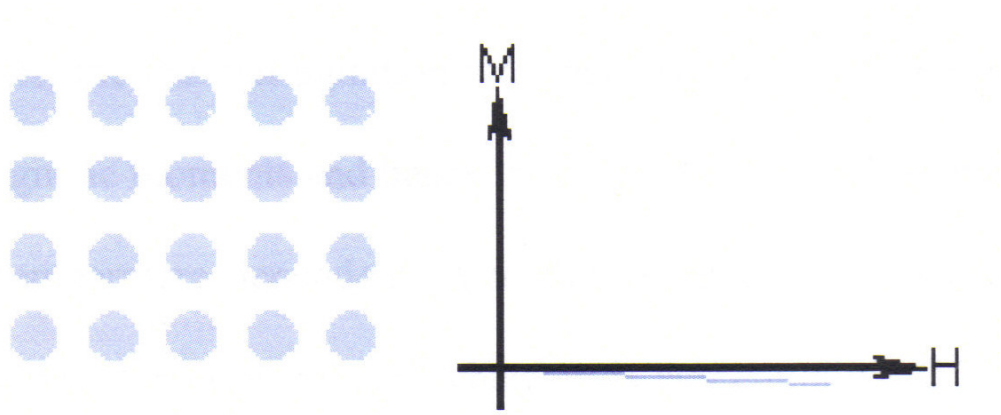


Figure 1.3 Atoms with no magnetic moment and small negative susceptibility

Diamagnetism is such kind of weak phenomenon that only the atoms with full-filled outer shells are classified as diamagnetic. The materials with stronger interactions are classified into other phenomenon such as paramagnetic or ferromagnetic.[1-6]

*1.2.2 Paramagnetism*

There are several theories of paramagnetism, which are valid for specific types of material. The Langevin model, which is for materials with non-interacting localized

electrons, states that each atom has a magnetic moment, which is randomly oriented as a result of thermal agitation (Figure l.4).

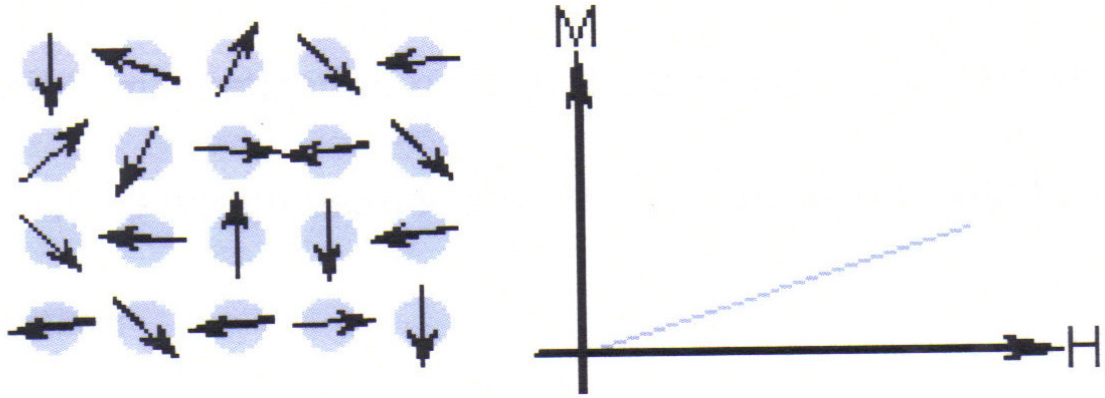


Figure 1.4 Atoms with randomly oriented moments and small, positive susceptibility.

For these class materials, some of the atoms or ions in the material have a net magnetic moment due to unpaired electrons in partially filled orbitals. However, the individual magnetic moments do not interact magnetically, and as with diamagnetism, the net magnetization is zero when the field is not applied. In the presence of a field, there is a partial alignment of the atomic magnetic moments in the direction of the field, resulting in a net positive magnetization such that the susceptibility $\chi$ is > 0 (order of $10^{-5}$ to $10^{-2}$) for paramagnetic materials.[1-3] In addition, the efficiency of an external field in aligning the moments is opposed by randomizing effects of the temperature. This results in a temperature dependent susceptibility known as the Curie Law.

*1.2.3 Ferromagnetism*

Ferromagnetic materials exhibit parallel alignment of permanent magnetic moments, resulting in a large net magnetization even in the absence of a magnetic field. These moments originate from the overall contribution of electron spin and orbital magnetic moments.[4] The elements Fe, Ni, and Co and many of their alloys are typical ferromagnetic materials. Magnetic susceptibility as high as $10^6$ is possible for ferromagnetic materials. Two distinct characteristics of ferromagnetic materials are their spontaneous magnetization and the existence of magnetic ordering temperature. The spontaneous magnetization is the net magnetization that exists inside a uniformly magnetized microscopic volume in the absence of an external field. As temperature increases, the arrangement of atomic moments is disturbed by the thermal agitation, resulting in temperature dependence of spontaneous magnetization. In spite of the presence of spontaneous magnetization, a large piece of ferromagnetic or ferromagnetic substance is usually not spontaneously magnetized but exists rather in a demagnetized state. This is because the interior of the piece is divided into many magnetic domains, each of which is spontaneously magnetized. Since the direction of domain magnetization varies from domain to domain, the resultant magnetization can be changed from zero to the value of spontaneous magnetization.[1] The saturation magnetization ($M_S$) is the maximum induced magnetic moment that can be obtained in a magnetic field beyond which no further increase in magnetization occurs. Saturation magnetization is an intrinsic property and dependent on temperature.

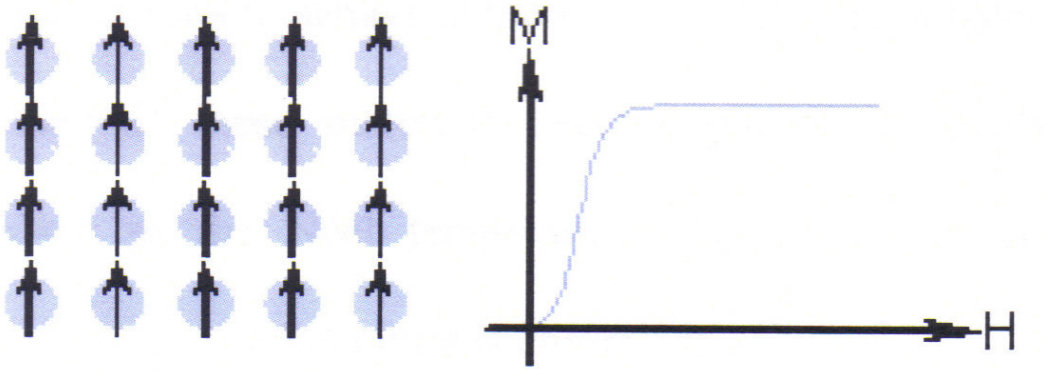


Figure 1.5 Atoms with parallel-aligned magnetic moments and the susceptibility is large and positive.

*1.2.4 Anti-ferromagnetism*

In some other types of materials, the magnetic moment coupling between adjacent atoms or Ions results in the anti-parallel alignment of the magnetic dipoles (Figure 1.6). This phenomenon of the alignment of spin moments of neighboring atoms or ions in exactly opposite directions is termed as anti-ferromagnetism, The opposing magnetic moments cancel one another, resulting in zero net magnetization of the material. [2,4] Some examples of anti-ferromagnetic crystals are manganese oxide (MnO), manganese sulfide (MnS), and iron oxide (FeO).

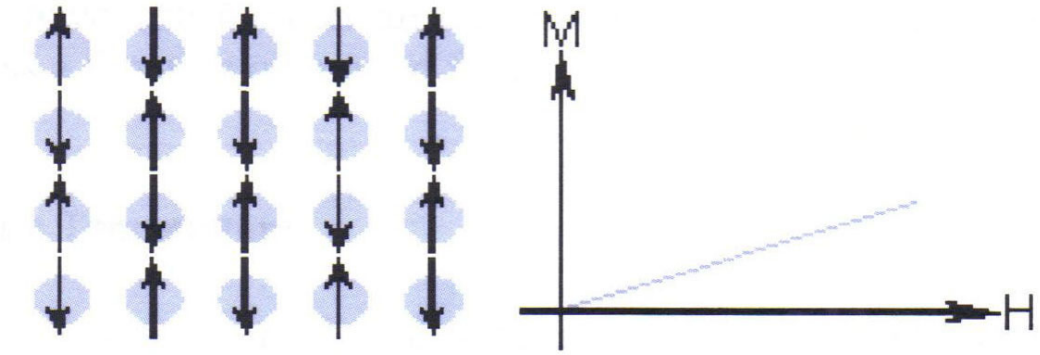


Figure 1.6 Atoms with anti-parallel aligned magnetic moments and the susceptibility is large and positive.

*1.2.5 Ferrimagnetism*

Ferrimagnetism is another type of magnetic ordering. In ferrimagnets, the moments of adjacent atoms or ions are in an anti-parallel alignment, but they do not cancel out each other (Figure 1.7). The best example of a ferromagnetic mineral is magnetite ($Fe_3O_4$). The structural formula for magnetite is $[Fe^{3+}]A\ [Fe^{2+},Fe^{2+}]BO_4$. This particular arrangement of cations on the A and B sublattices is called an inverse spinel structure. With negative AB exchange interactions, the net magnetic moment of magnetite is due to the B-site $Fe^{2+}$ because the moments from the trivalent ions are opposite and cancel each other. Ferrimagnetism is therefore similar to ferromagnetism. Ferrimagnetism exhibits all the hallmarks of ferromagnetic behavior: spontaneous magnetization, Curie temperatures, hysteresis, and remanence. However, ferromagnets and ferrimagnets have very different magnetic ordering.

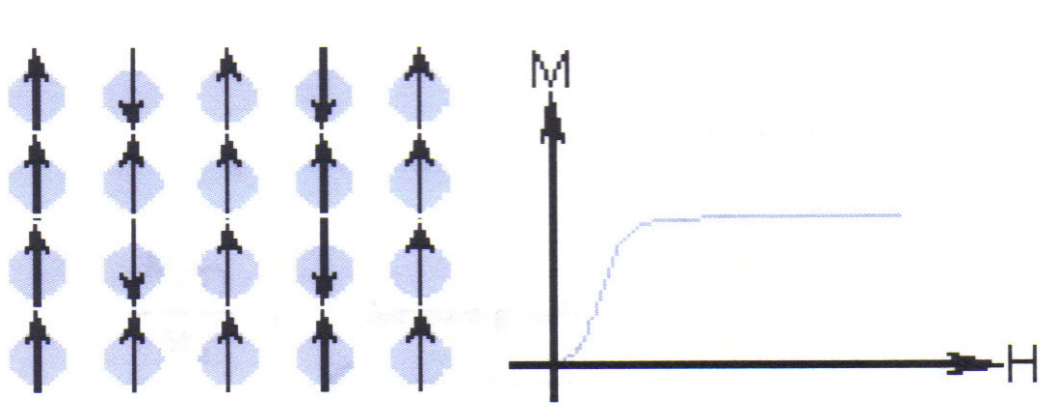


Figure 1.7 Atoms with the mixture of parallel and anti-parallel magnetic moments and the susceptibility is small and positive.

## 1.3 Characteristic of Ferromagnetic Materials

### *1.3.1 Curie Temperature*

Even though electronic exchange forces in ferromagnets are very large, thermal energy eventually overcomes the exchange interaction and produces a randomizing effect. This effect becomes dominant at a particular temperature called the Curie temperature ($T_c$). Below the Curie temperature, the magnetic structure is ordered, and above the Curie temperature the magnetic structure is disordered. The saturation magnetization goes to zero at the Curie temperature. The magnitude of the Curie temperature varies from material to material. At $T_c$ the mutual spin coupling forces are completely destroyed, such that for temperatures above $T_c$ both ferromagnetic and antiferromagnetic materials are paramagnetic (Figure 1.8). The Curie temperature is an intrinsic property of materials and is a diagnostic parameter that can be used for mineral

identification. However, it is not full proof because different magnetic minerals, in principle, can have the same Curie temperature.

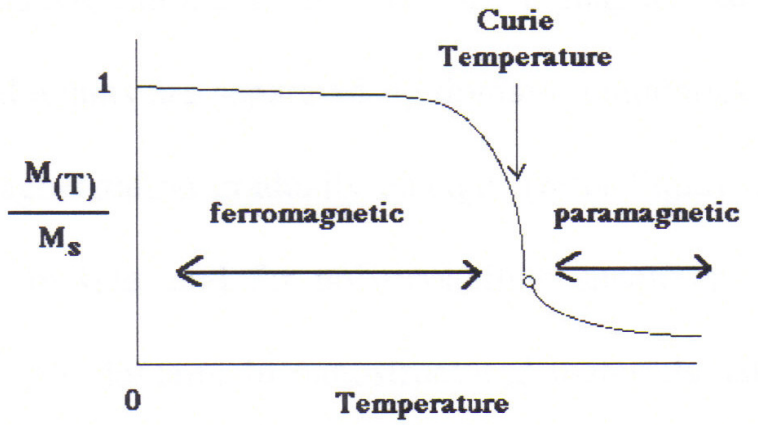


Figure 1.8 Typical temperature dependence of a ferromagnetic.

*1.3.2 Magnetic Anisotropy*

In many situations, the susceptibility of a ferromagnetic material will depend on the direction where it is measured. Such a situation is called magnetic anisotropy. When magnetic anisotropy exists, the total magnetization of a ferromagnetic $M_s$ will prefer to lie along a special direction called the easy axis. There are several causes of anisotropy, including those induced by stress and prior mechanical handling of materials. Two important and common sources of anisotropy, which are magnetocrystaillne anisotropy and shape anisotropy, are discussed below.

1.3.2.1 Magnetocrystalline Anisotropy

Only megnetocrystalline anisotropy, or simply crystal anisotropy, is intrinsic to the materials; all other anisotropies are induced. In crystal anisotropy, the ease of

obtaining saturation magnetization is different for different crystallographic directions. The direction of easy magnetization of crystal is the direction of spontaneous domain magnetization in the demagnetized state. In case of hexagonal close packed (HCP) or tetragonal crystal, the easy axis is usually the c-axis. Under an applied field, the magnetic moment deviates from the easy direction and returns to its original alignment with the removal of the field. The energy associated with this alignment is called the anisotropy energy and in its lowest order form is given by:[2]

$$E_a = K \sin^2 \theta \tag{1.5}$$

where $\theta$ is the angle between $M_s$ and the easy axis, and K is the anisotropy constant (units is ergs/cm$^3$). The examples are single crystal iron and cobalt as shown Figure 1.9.

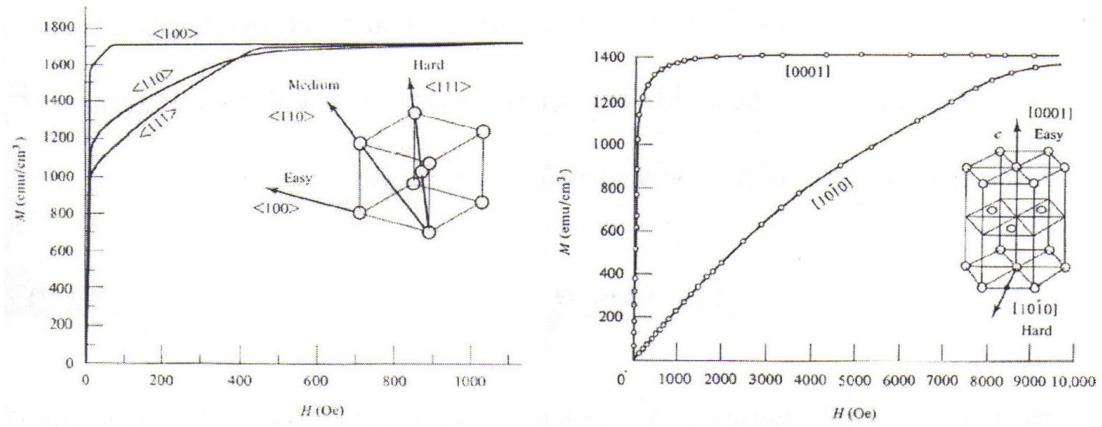


(a) (b)

Figure 1.9 Direction dependence of magnetization (a) iron, and (b) Cobalt[2]

1.3.2.2 Shape Anisotropy

It is easier to induce a magnetization along the long direction of a nonspherical piece of material than along a short direction. This is so because the demagnetizing field

is less in the long direction, for the reason that the induced poles at the surface are farther apart. Thus, a smaller applied field will negate the internal, demagnetizing field. The shape anisotropy can be very important for non-spherical materials. The long axis of a specimen plays the same role as the easy axis of the crystal, and the shape anisotropy constant $K_s$ is given by:

$$K_s = 1/2(N_a - N_c)M^2 \qquad (1.6)$$

Magnetization is easy along the c-axis and equally hard along any axis normal to c (assume a). If c decreases until it equals a, the specimen becomes spherical ($N_a = N_c$. $K_s = 0$) and shape anisotropy disappears. [2]

*1.3.3 Magnetic Domain*

Any ferromagnetic material at a temperature below Curie temperature ($T_C$) is composed of small-volume regions known as domains, in which there is the mutual alignment of the magnetic moments in the same direction, as illustrated in Figure 1.10(a). Each domain is magnetized to its saturation magnetization and adjacent domains are separated by domain walls (Blochwalls), across which the direction of magnetization gradually changes. (Figure 1.10(b)).

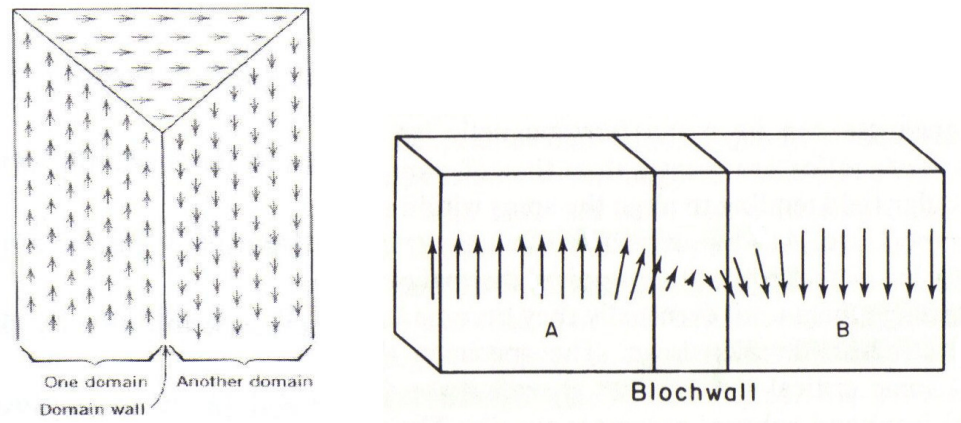


**(a)** **(b)**

Figure 1.10 (a) Creation of domain and domain wall and (b) Spin orientation rotation through domain (Bloch) wall.[4]

Bloch walls are not always rigidly fixed and it can move though the samples. It means that one domain may be enlarged in volume whereas another one may reduce, as shown in Figure 1.11. One method to cause domains increasing is to apply an external magnetic field on the specimen.[4]

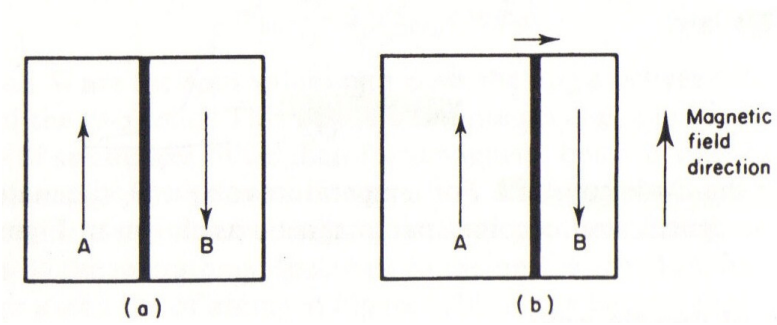


Figure 1.11 The movement of domain wall cause by the application of an external magnetic field.[4]

*1.3.4 Hysteresis Loops*

Ferromagnets can retain the memory of an applied field even after the field is removed. This behavior is called hysteresis, and a plot of the variation of magnetization with magnetic field is called a hysteresis loop. The hysteresis loop is a means of characterizing magnetic materials, and various parameters can be determined from it.

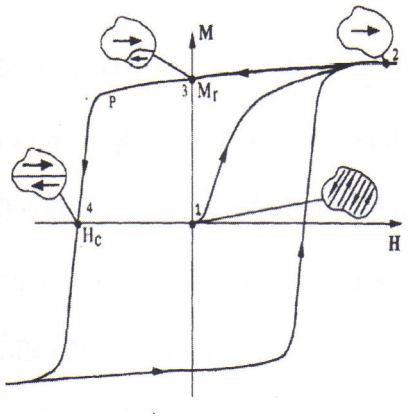


Figure 1.12 The magnetization curve and hysteresis loop of a permanent magnet showing the virgin state (1), at saturation (2), at remanence (3), and at the coercive field (4).[9]

Initially, the moments of the constituent domains are randomly oriented in such a way that there is no net B (or M) field. As shown in Figure 1.12, on the application of a field to an un-magnetized sample, the polarization increases initially by the growth of favorably oriented domains, which will be magnetized in the easy direction of the crystal. When the polarization can increase no further by the growth of domains, the direction of magnetization of the domains then rotates away from the easy axis to align with the field. When all of the domains have fully aligned with the applied field, saturation is reached, and the polarization can increase no further. The maximum value

of M is called the saturation magnetization $M_s$, and the resultant M-H curve is called the initial magnetization curve. Starting from the saturation point (see Figure 1.12), when the H field is reduced, the curve does not retrace its original path. A hysteresis effect is produced in which the M field lags behind the applied H field or decreases at a lower rate. At zero field, a residual M is called the remanence or remanent magnetization $M_r$ is retained, indicating that the material remains magnetized even in the absence of an external H field. The polarization will only decrease after a sufficiently high field is applied to: (1) nucleate and grow domains favorably oriented with respect to the applied field or (2) rotate the direction of magnetization of the domains towards the applied field. After applying a high enough reversal field, saturation polarization will be achieved in the negative direction. If the applied field is then decreased and again applied in the positive direction then the full hysteresis loop is plotted (Figure 1.12). The area contained within the loop indicates the amount of energy absorbed by the material during each cycle of the hysteresis loop. The reverse field required to bring the magnetic induction B of a specimen to zero is called the inductive coercivity ($H_b$) whereas the reverse field required to bring the magnetization M to zero is called the intrinsic coercivity ($H_c$). The remanence ratio $M_r/M_s$ is generally used as measure of squareness of the M-H loop.

Maximum Energy Product $(BH)_{max}$ : In B-H loop, the maximum value of the product of B and H is called the maximum energy product, ($(BH)_{max}$) and is a measure of the maximum amount of useful work that can be performed by the magnet. Its unit is $KJ/m^3$ (MGOe). For a permanent magnetic material, the $(BH)_{max}$ is twice the maximum

magnetostatic energy available from a magnet of optimal shape. The product tends to increase with both increasing coercive field $H_c$ and saturation magnetization $M_s$. However, for materials with sufficiently high $H_c$ values ($H_c > 2\pi M_s$) , the theoretical limit for the energy product is limited only by Ms and is given by:[11]

$$(BH)_{max} \leqq (2\pi M_s)^2 \tag{1.7}$$

*1.3.5 Soft Magnetic Materials*

Soft magnetic materials can be easily magnetized and demagnetized by low-strength magnetic field. When an applied field is removed, soft magnetic materials will return to a state of relatively low residual magnetization. Soft magnetic materials are used primarily to enhance or channel the flux produced by an electric current. The main parameter, which is often used as a figure of merit for soft magnetic materials, is the relative permeability, which is a measure of how readily the material responds to the applied magnetic field. The other main parameters of interest are the coercivity, the saturation magnetization, and the electrical conductivity. As shown in Figure 1.13, typical soft materials have very low intrinsic coercivity and high saturation magnetization $M_s$ but low $M_r$.

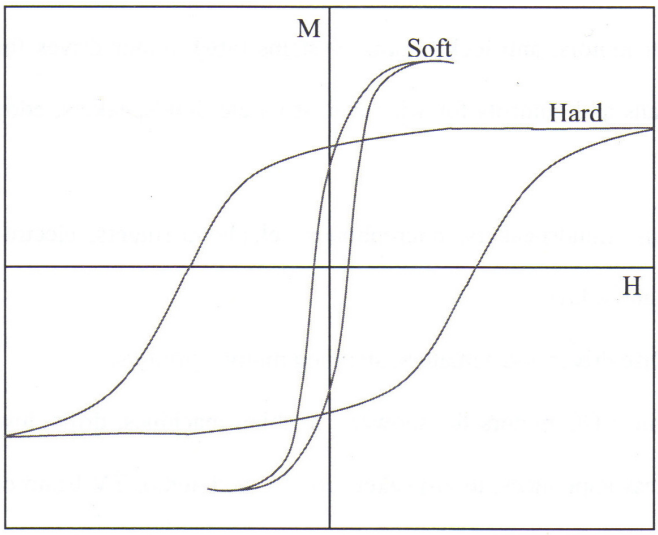


Figure 1.13 M-H curves for soft hard magnets.

*1.3.6 Hard Magnetic Materials*

Hard magnets, also referred to as permanent magnets, are magnetic materials that can retain their magnetism after being magnetized. The term "hard" is used to describe materials that have sufficiently high resistance to demagnetizing field. Coercivity is therefore the key to distinguishing between hard and soft phase magnetic materials. As shown in Figure 1.13, materials that have an intrinsic coercivity of greater than 1000 Oe and typically high remanence $M_r$ are hard magnetic materials. Such material has high energy product $(BH)_{max}$, which is the figure of merit of permanent magnet.

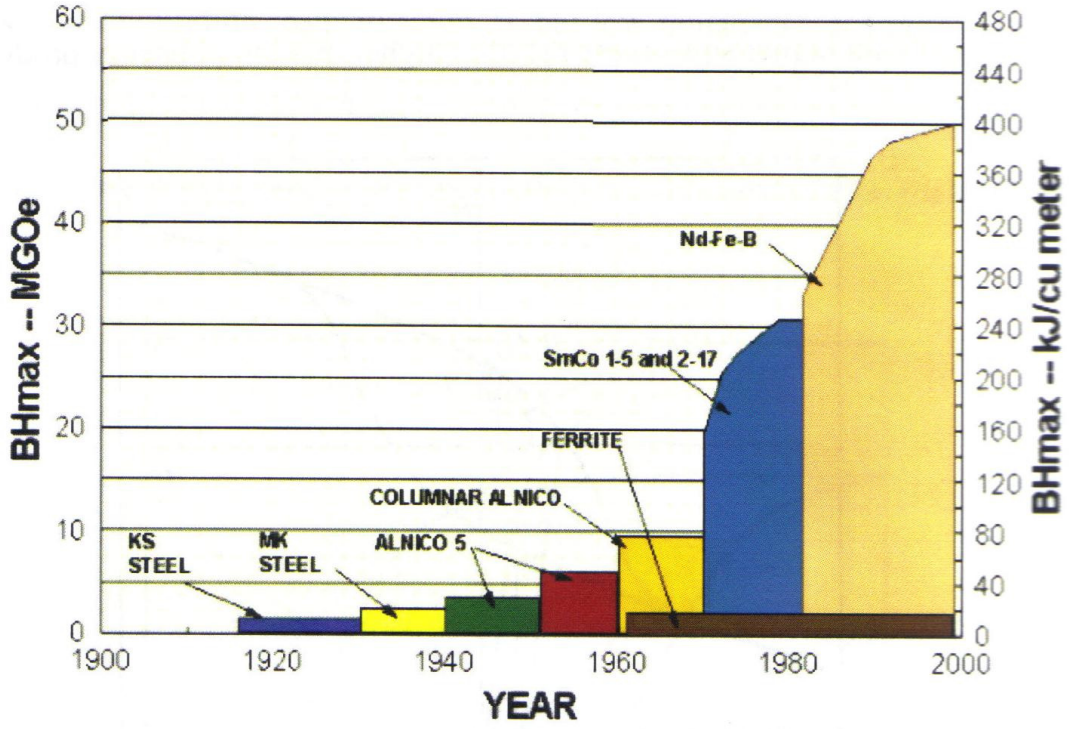


Figure 1.14 Evolution of $(BH)_{max}$ of permanent magnets in 20th century[10].

*1.3.7 Exchange-coupled Hard/Soft nanocomposite Magnets*

Driven by the limitation in equation (1.5) $(BH)_{max} \leqq (2\Pi M_s)^2$, research has been focused on developing new high-anisotropy materials with high $M_s$ and Curie temperature ($T_c$). Thus, new hard-magnetic compounds such as $SmCo_5$, $Sm_2Co_{17}$, and $Nd_2Fe_{14}B$ are made. Unfortunately, these compounds still have magnetization values significantly lower than that of Co, Fe, or $Fe_{65}C_{O35}$, which have $4\pi M_s$ values of 18, 21, and 24 kG, respectively.[11] In 1991, Kneller and Hawig[12] proposed an alternative approach to enhance the transition metal content to increase $M_s$ by making a nanocomposite of exchange-coupled hard and soft magnetic phases. Such magnets are

referred as exchange-spring magnets and provide a new approach to increased $(BH)_{max}$. The hard phase provides the requisite magnetic anisotropy and stabilizes the exchange-coupled soft phase against demagnetization, and the soft phase provides the high magnetization (as shown in Figure 1.15).[13-15]

Exchange-coupled nanocomposite was first observed by Coehoorn et al.[16] in a melt-spun $Nd_{4.5}Fe_{77}B_{18.5}$ sample that, when annealed, consisted of a mixture of $Nd_2Fe_{14}B$, $Fe_3B$, and Fe phases. Skomski and Coey explored the theory of exchange-coupled films and predicted that a giant energy product of 120 MGOe might be attainable by exploiting the exchange-spring mechanism in oriented nanostructured magnets.[17-19] It has also been predicted that, for effective exchange coupling, the grain size of soft phase should not be larger than twice the domain-wall thickness of hard phase. Future applications of exchange-spring magnets will likely be based on a nanoscale dispersed composite geometry obtained in bulk processing.[19-21]

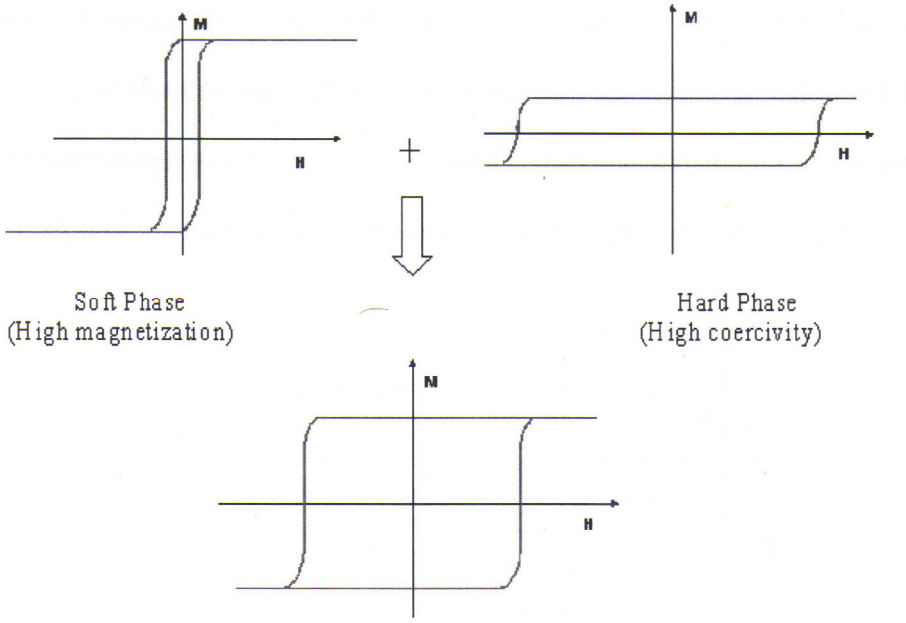


Figure 1.15 Hysteresis loops of soft, hard, and hard/soft nanocomposite magnets.

# CHAPTER 2

## MAGNETIIC NANOPARTICLES

Magnetic nanoparticles exhibit a drastically different properties compared to from those of their bulk counterparts because of the high surface to volume ratio of the particles at nanometer scale. Magnetic properties of small ferromagnetic particles, such as coercivity and saturation magnetization, are mainly dominated by two key features: (1) a size limit below which the specimen cannot be broken into domains, and so it remains with single domain; and (2) the thermal energy in small particles, which decouples the magnetization from the particle itself to give rise to the phenomenon of superparamagnetism. These two key features are represented by two key sizes (on the length scale): the single domain size and the superpararnagnetic size as shown in figure 2.1.[2,9]

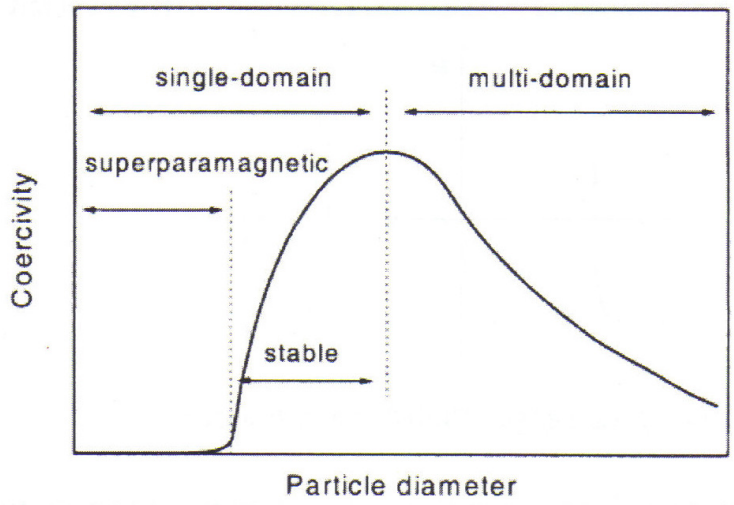


Figure 2.1 Variation of coercivity with particle diameter.

## 2.1 Single-Domain Particles

The magnetostatic energy of a ferromagnet could be decreased by restructuring the material into domains. There is a limit to this because the formation of domains costs energy as a result of domain wall formation. Thus, in a large body there could be minimum domain size below which the energy cost of domain formation exceeds the benefits of decreasing the magnetostatic energy. When the size of the magnets decreases to a critical particle diameter, the formation of domain walls is energetically less favorable, and the magnets have only a single domain. Magnetization reversal in single-domain particle occurs via spin rotation, since there are no domain walls to move. Single-domain particles consequently have a larger coercivity compared to multi-domain system as it is harder to rotate the magnetization than to move a domain wall.[2,9]

In this single-domain regime, the magnetic coercivity increases as the size of the nanoparticle increases with the relationship:

$$H_c = 2K/m_s[1- 5(k_B T/KV)^{1/2}] \quad (2.1)$$

where $M_s$ is the saturation magnetization.[22] Above the critical size ($D > D_C$), multi-domain magnetism begins in which a smaller reversal magnetic field is required to make the net magnetization zero.

Saturation magnetization of nanoparticles is also strongly dependent on their size. Magnetic materials intrinsically possess magnetically disordered spin glass-like layers near the surface due to the reduced spin-spin exchange coupling energy at the surface.[23,24] In bulk cases, since the disordered surface layer is minimal compared to the total volume of the magnet, such surface spin canting effects are negligible. Upon reduction of the size of magnetic materials to the nanoscale regime, however, the surface canting effects are dramatically pronounced in the saturation magnetization value ($m_s$) , described as:

$$m_s = M_s[(r - d)/r]^3 \quad (2.2)$$

where $r$ is the size; $M_s$ is the saturation magnetization of bulk materials, and d is the thickness of disordered surface layer.[23] For very small nanoparticles (less than ~5 nm) such size effect on $m_s$ is more noticeable, since internal spins of the nanoparticles also start to be canted as do the surface spins because of increased interactions between the surface and internal spins.[23]

## 2.2 Superparamagnetism

Superparamagnetism is a phenomenon by which magnetic materials may behave similar to paramagnetism at temperatures below the Curie or the Neel temperature. It occurs when the materials are composed of very small crystallites (usually below 10nm). In this case, even though the temperature is below the Curie or Neel temperatures, the thermal energy is sufficient to overcome the coupling forces between neighboring atoms, leading to change in the direction of magnetization of the entire crystallite. The resulting fluctuations in the direction of magnetization cause the magnetic field to average to zero. The material behaves in a manner similar to paramagnetism, except that instead of each individual atom being independently influenced by an external magnetic field, the magnetic moment of the entire crystallite tends to align with the magnetic field. The energy required to change the direction of magnetization of a crystallite is called the crystalline anisotropy energy (KV) and depends both on the material properties and the crystallite size. As the crystallite size decreases, so does the crystalline anisotropy energy, resulting in a decrease in the temperature at which the material becomes superparamagnetic.[2,9] A typical hysteresis loop of superparamagnetic nanoparticles is shown in Figure 1.9 with $H_c = 0$ and $M_r/M_s = 0$

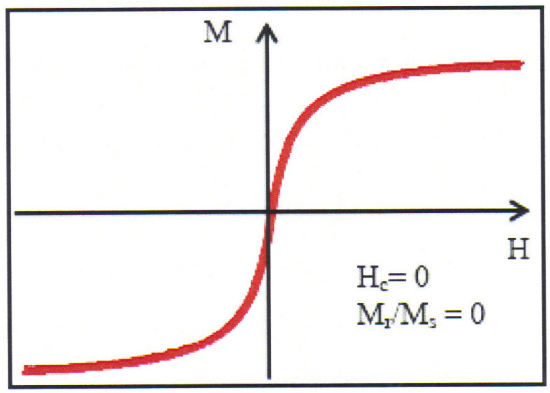


Figure 2.2 Typical magnetization curve of supermagnetic materials.

The phenomenon of superparamagnetism is timescale-dependent due to the stochastic (random variable) nature of the thermal energy. The time scale for successful jump can be calculated by

$$\tau = \tau_0 e^{-KV/k_B T} \tag{2.3}$$

Where attempt timescale ( $\tau_0$) is about $10^{-9}$s and V is the volume of particle. This equation (2.3) describes the time scale over which the moment of particles ( $\mu p = M_s V$) attempts to jump the anisotropy energy (KV) barrier. Typical experiment with a magnetometer takes 10 to 100 s; if $M_s$ reversed at times shorter than the experimental timescale, the system appears superparamagnetic. Using $\tau$ = 100 s and $\tau_0 = 10^{-9}$ S ,we can obtain the critical volume from equation (2.4)

$$V_{sp} = 25 k_B T/K \tag{2.4}$$

A particle with a volume smaller than this quantity acts superparamagnetically on the 100 s experimental timescale. Equation (2.5) can be rearranged to yield

$$T_B = KV/25k_B \quad (2.5)$$

$T_B$ is called the blocking temperature; below $T_B$ the free movement of moment of particles ( $\mu_p = M_s V$) is blocked by the anisotropy; above $T_B$, k kicks the moment loose so that the system appears superparamagnetic.

## 2.3 Synthesis of Magnetic Nanoparticles

A series of general methods for the magnetic nanoparticle synthesis have now been developed.[20] An essential feature of their synthesis is the preparation of particles of specified size and shape (at least, the size distribution should be less than 5~10%, and controllable), The shape control and the possibility of synthesis of anisotropic magnetic structures are especially important. In order to eliminate (or substantially decrease) the interparticle interactions, magnetic nanopartlcles often need to be isolated from one another by immobilization on a substrate surface or in the bulk of a stabilizing inert matrix. It is important that the distance between the particles in the matrix should be controllable, finally, the synthetic procedure should be relatively simple, inexpensive and reproducible. The methods of generation of magnetic nanoparticles in the gas or solid phase using high-energy treatment of the material are usually called physical, while trenanopar1lcle syntheses, which are often carried out in solutions at moderate temperatures are chemical methods.

*2.3.1 Physic Methods*

2.3.1.1 Condensation Methods

The method of nanoparticle synthesis from supersaturated metal vapors is based on the classical nucleation theory where the nascent phase clusters are described by the spherical liquid drop model. Nanoparticles (clusters) are prepared using various ways of metal evaporation: laser vaporisatlon,[21, 25] thermal vaporisation,[26,27] arc discharge, plasma vaporisation,[28] and solar energy-induced evaporatlon.[29] In each method, special installations are employed differing in engineering solutions of particular units.[30]

For example, in the classical thermal vaporization method, a metal or alloy sample is heated in a tungsten boat in an argon or helium stream. The atoms of the vaporized metal lose kinetic energy upon collisions with inert gas atoms, gather in clusters and condense on a cooled substrate as a nanodispersed powder. By varying the evaporation rate, the substrate temperature and gas pressure and composition, one can control the particle size in the 100±3 nm range. Most often, prior to opening the installation and taking out the sample, nanoparticles are passivated by passing an inert gas/ oxygen mixture for several minutes. In particular, this method has been used to prepare heterometallic nanoparticles (~30 nm) with the composition Fe-M (M=Ni, Mn, Pt, Cr).[26]

2.3.1.2 Mechanical Milling

The mechanochemical dispersion of a compact material in mills of various designs appears an attractive way to produce disperse systems. However, there exists a mechanical dispersion limit for solids,[31,32] which prevents in some cases the preparation

of nano-sized particles with a narrow dispersion. In addition, high energy impact on the material being ground result in intensive interaction of the nanoparticles formed with the dispersion medium. The morphology of the nanoparticles can be controlled by changing milling speed, time, type and size of grinding medium (balls), milling media, milling temperature etc.

*2.3.2 Chemical Methods*

Diverse metal-containing compounds (MCC) including metal carbonyls, organometallic compounds, metal carboxylates, etc., are used as the precursors in the chemical synthesis of magnetic nanoparticles. Most often, precursors decompose on heating or UV irradiation; other types of treatment of MCC, resulting in nanoparticles, have also been developed.

2.3.2.1 Electrochemical Generation

This method is used as a method for the synthesis of substantial amounts of rather small(~2 nm) nanoparticles with a narrow dispersion.[33] A standard electrochemical cell containing an alcohol solution of tetraalkylammonium halide was used to obtain cobalt particles. On passing the current, the cobalt anode dissolved to give Co nanoparticles near the cathode (glass carbon). The influence of electrolysis conditions on the magnetic characteristics of the resulting nanopartices was studied using several examples. The average size of a particle formed upon electrochemical dispersion was inversely proportional to the current density. Evaporation of the solvent yields crystallites, which can be readily converted again into a colloid suspension.[34]

2.3.2.2 Thermal Decompositions of Metal-containing Compounds

Thermal decomposition of metal-containing compounds has been studied in detail in relation to the development of the scientific grounds of the metal organic chemical vapor deposition (MOCVD) technique, which is used successfully to obtain nanoparticles. When the reaction is carried out in a liquid medium in the presence of surfactants or polymers, it is possible to stabilize the resulting amorphous nanoparticles with diameters of up to 10 nm. An interesting example of two-stage thermolysis of $Fe(CO)_5$ has been reported.[35] First, an iron oleate complex is formed from $Fe(CO)_5$ and oleic acid at 100°C; at 300°C, the complex decomposes to give primary 'loose' nanoparticles (11 ± 4 nm). After maintaining at 500°C, these are converted, as shown by powder X-ray diffraction, into crystalline $\alpha$-Fe nanoparticles. Laser photolysis of volatile MCC (most often, metal carbonyls) is also suitable for this purpose.[36]

2.3.2.3 Ultrasonic Decomposition of Metal-containing Compound

In this method, metal carbonyls and their derivatives are used as metal-containingcompounds, although cases of successful use of other organometallic compounds are also known. Nanoparticles are synthesized by ultrasound-induced decomposition of a solution of MCC in solvent. In order to retain the monodispersity and prevent aggregation of the particles formed, suitable surfactant is added to the solution.[37]

2.3.2.4 The Reduction of Metal-containing Compounds

Magnetic metallic nanoparticles can be prepared from metal salts using strong reducing agents, namely, alkali metal dispersions in ethers or hydrocarbons, alkali metal

complexes with organic electron acceptors (e.g., naphthalene), 1,2-hexadecanediol (HDD) and other complex hydrides. By using HDD in aqueous solutions at room temperature, both homo- (Fe, Co, Ni) and heterometallic(CoFe, FeCu, CoCu) nanoparticles were obtained as amorphous powders. High-boiling alcohols are also used as reducing agents. The reduction of cobalt acetate with dodecane-1 ,2-diol at 250°C in oleic acid in the presence of trioctylphosphine gives $8 \pm 3$ nm Co particles.[38] nickel-containing nanoparticles have been prepared in a similar way.[39]

2.3.2.5 Sol-gel Method

The sol-gel method is widely used in a number of technologies.[40] In nanotechnology, it is used most often to obtain metal oxides but is also applicable to the synthesis of nanosized metals and fused bimetallic and heteroelement particles. For example, reduction of $Ni^{2+}$ and $Fe^{2+}$ ions inserted in silica gel in 3 : 1 ratio with hydrogen resulted in $Ni_3Fe$ nanoparticles ($19 \pm 4$ nm) within the $SiO_2$ matrix.[41]

# CHAPTER 3

# MAGNETIIC NANOWIRES

A nanowire is a nanostructure which has large aspect ratios between length and diameter. Nanowires may have diameters in a range of 1-200nm and an unconstrained length.

The magnetic properties of the materials becomes strongly size dependent in nanometer size range. With weak crystalline anisotropy, magnetic properties may mainly controlled by shape anisotropy. For magnetic nanowire, it will be easy to rotate if the magnetization is along the long axis than if is along one of the short axes. This produces an easy axis of magnetization along the long axis. In larger sized particles, shape anisotropy is less important than smaller size particles.

## 3.1 Synthesis of Magnetic Nanowires

A series of methods to synthesize magnetic nanowires have now been developed. In order to obtain materials with higher magnetic properties, the possibility to synthesize an anisotropic magnetic structure and the shape control are very important. The methods of nanowires synthesis which are often carried out in solution at moderate temperatures are usually call chemical, and the generation of nanowires in the gas or solid phase with high energy treatment of the materials are physical method.

In this section, the methods are mainly about "bottom-up" approaches, which afford many kinds of nanowire in huge numbers, and don't need highly sophisticated equipments.

*3.1.1 Physic Methods*

3.1.1.1 Physic Vapor Deposition (PVD)

In this method, the target consisting of the material to be deposited is bombarded by a high energy source such as a beam of electrons or ions. The atoms from the surface of target are vaporized and introduced though the pores of the template and cooled to solidify. For example, by using an especially designed experiment setup, nearly single-crystal Bi nanowires in anodic aluminum templates with pore diameters in 7 nm have been synthesized. These Bi nanowires were found to process a preferred crystal growth orientation along the wire axis. [42]

3.1.1.2 Stress-Induce Growth

Cheng et al. grew bismuth nanowires by this method in 2002. The nanowires presumably grow from the defects and cleavage fractures in the sputtered films of layers of Bi and CrN, and the length are up to several millimeter with the range of diameters from 30 to 200 nm. [43] While the research of this technique has only begun, stress-induced unidirectional growth should be applied to a variety of composite films.

3.1.1.3 Pressure Injection

The pressure injection technique is often applied to fabricate highly crystalline nanowires from a low-melting point material or by using porous templates with robust mechanical strength. In this method, The target material in liquid form is pressure-

injected into the evacuated pores of the template and form nanowires. Due to the high pressures and temperature, the templates used for the pressure injection method should be chemically stable and maintain the structure at high temperature and high pressure. Anodic aluminum oxide films and nano-channel glass are two types of materials used as templates in this technique. By using this method, metal nanowires (Bi, In, Sn and Al) and semiconductor nanowires (Se, Te, GaSb, and $Bi_2Te_3$) have been synthesized in anodic aluminum oxide templates.[44,45,46]

*3.1.2 Chemical Methods*

3.1.2.1 Template Synthesis

In template-assisted synthesis method, it is very important to consider the chemical stability and mechanical properties of the template. The diameter, uniformity and density of pores will affect the properties of nanostructures. The most popular templates used in nanowires fabrication include anodic alumina ($Al_2O_3$), nano-channel glass, ion track-etched polymers and mica films.

Anodic alumina templates are fabricated by anodizing pure Al films in different acids.[47,48,49] The result of oxide films are regular hexagonal array of parallel and nearly cylindrical channels. The uniform diameter pores formed because of a balance between electron-field-enhanced diffusion which controls the growth rate of the alumina, and dissolution of the alumina into acidic electrolyte.[50] Depending on the synthesis condition, the pore diameter can be systematically controlled from $<$ 10nm up to 200nm with a pore density in a range from $10^9$ to $10^{11}$ pores/cm$^2$.[51,52]

In nanowires synthesis, the template itself can be used in a variety of deposition processes. The template pore is used both to pattern the structures and provide a site where chemistry takes place. The template is broadly applied on different chemistry methods such like Electrochemical deposition, chemical vapor deposition and vapor-solid-liquid to fabricate nanowires.

3.1.2.2 Electrochemical Deposition

The electrochemical deposition technique has widely studied for fabricating nanowires. It does not require a special environment (vacuum, high pressure or high temperature). The equipment and chemicals are relatively inexpensive depending on the materials that are being deposited in the pores of the template. Traditionally, this method is used to grow thin film on conducting surface. Since electrochemical growth is usually controlled in the direction normal to substrate surface, this method is really can be applied on fabricating 1D or 0D nanostructures. This method has been widely applied to synthesize metals and semiconductors nanowires., such like Co[53,54], Ni[53,55], Fe[56], Cu[57,58], Ag[59] and CdS[60].

In this method, a thin conducting metal film is coated on one side of the porous membrane to be the cathode for electroplating. The length of the deposited nanowires can be controlled by adjusting the duration of the electroplating process. The chosen template for electrochemical deposition should be chemically stable during the electrolysis process. Defects and cracks in the templates are detrimental to nanowires growing, in this reason, the deposition processes primarily occur in the more accessible cracks. Particle track-etched mica film or polymer membranes are typical templates

used in simple dc electrolysis. In order to use anodic aluminum oxide films in the dc electrochemical deposition,[61] the insulating barrier layer which separates the pores from the bottom aluminum substrate have to be removed. The nanowires which fabricated in electrochemical composition method are no preferred crystal orientation.

One of advantaged of the electrochemical deposition method is the possibility to fabricate multi-layered structures within nanowires. By controlling the cathodic potentials of electrolye which contains two different kinds of ions, different metal layers can be deposited.

3.1.2.3 Chemical Vapor Deposition (CVD)

There are two chemistry methods to fabricate nanowires in vapor deposition technique, chemical vapor deposition (CVD)[62] and Metallogranic chemical vapor deposition (MOCVD).[63] Like electrochemical deposition, vapor deposition is usually able to synthesize smaller-diameter ($\leqq$ 20nm) nanowires than pressure injection methods.

In typical CVD process, the catalysts (usually metal nanodroplets) was coating on the substrate and exposed to one or more volatile precursors, which react or deposit on the catalyst and form the desire nanowires.

For example, ZnS nanowires were grown on gold (Au) coated silicon substrates through a simple chemical vapor transport-condensation (CVTC) based on the vapor–liquid–solid (VLS) mechanism. The Au film at high temperature breaks up and liquid Au nanodroplets were formed on the Si surface. These liquid Au droplets absorb ZnS vapor and formed Au–ZnS alloys. When the concentration of ZnS in the alloy is over

the saturation point, the ZnS alloy precipitates from the solid–liquid interface. ZnS nanowires originate from these precipitates.[64]

3.1.2.4 Vapor-Liquid-Solid methods (VSL)

Recently, some of successfully fabricated semiconductor nanowires are base on the vapor-liquid-solid (VSL) method. This is a mechanism for one-dimensional nanostructures growing. The growth of nanocrystals which directly adsorb a gas phase on to a solid surface is generally very slow. The mechanism of VLS is using catalyst such like liquid alloy phase which can rapidly adsorb a vapor to supersaturation levels, and the nucleation generates a solid precipitate of the source material. These seeds become the preferred site for material deposition at the interface of the liquid droplet. The seeds will elongate into nanowires or whiskers. The deposit which anisotropy is like a whisker whose diameter is controlled by the diameter of the liquid alloy droplet.

3.1.2.5 Solution-Phase Synthesis

Solution-phase synthesis is a method to control the diameter of nanowires without using templates, catalysts, or surfactant. Gates et al. made use of the anisotropy of the crystal structure which can be viewed as rows of 1D helical atomic chains.[65,66] Their approach is based on the mass transfer of atoms during an aging step from a high free-energy solid phase to form a seed which grows preferentially along one crystallograohic axis. The diameter of the seed which is related to the diameter of the nanowire can be controlled by the temperature of the nucleation step.[67]

However, it is necessary to use surfactants to improve the anisotropic 1D growth of nanocrystals. Surfactants can stabilize the interfaces of nanoparticles and prevent

oxidation and aggregation processes.[68] The researches on the effect of growth conditions showed that they can be operated to induce a directional growth of the nanocrystals, usually generating nanorods, and in certain cases, nanowires of high aspect ratio. Manna et al. used a mixture of two surfactants to grow CdSe nanorods, and the concentration ratio of surfactants influenced nanocrystal structure. It is believed that the different surfactants have different affinities and different absorption rates for the different crystal faces of CdSe, thereby controlling growth rate of these faces.[69] Bashouti et al. used alkyl-diamine solvent to grow polycrystalline PbSe nanowires at low temperature.[70] The surfactant-induced direction growth is believed to occur, due to the formation of organometallic complexes in which the bidentate ligand assume the equatorial positions, thus hindering the ions from approaching each other in this plane. Furthermore, the alkyl-amine molecules can coat on the external surface of nanowires and prevent lateral growth.

## 3.2 Nanowire Growth and Nucleation

There are two important processes in the growth of nanocrystals in solution, the nucleation and the growth of the nanocrystals. The discussion of these two processes is in the following two subsections.

### *3.2.1 Theory of Nucleation*

La Mer et al. had study of extensively nucleation and growth in sulfursols[71,72], from the research they developed and explained the mechanism for the formation of colloids and nanocrystals from a supersaturated, homogeneous medium.

The mechanism is that the colloid synthesis should be designed in such a way that the concentration increases rapidly, then rising above the saturation concentration for a short period, and a burst of nucleation occurs with the formation of lots of nuclei in a short time. These particles grow rapidly and decrease the concentration below the nucleation level which allows the particles to grow at the rate limited by the slowest step in the growth process. By this way, the nucleation and growth of nanoparticles can be separated in time. Figure 3.1 shows the simple diagram of La Mer's mechanism. The high nucleation rate is leading to the burst of nuclei formation in a short time. These nuclei grow in a fast rate and reduce the concentration below the concentration level of rapid nucleation, and the slow growth rate leading to a longer growth period.

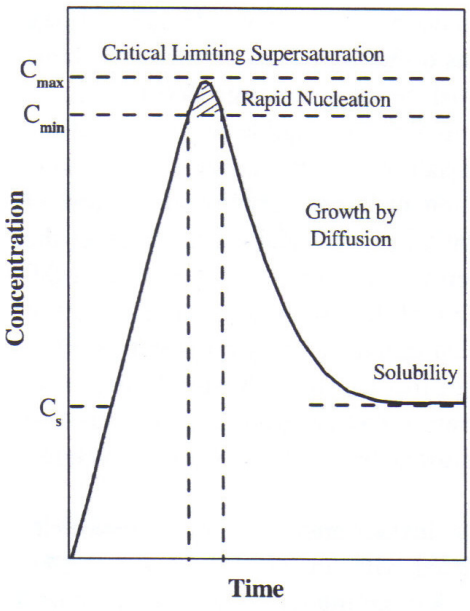


Figure 3.1 The illustration of La Mer's condition for nucleation.

The key idea of separating nucleation stage and growth process in time is to obtain the monodisperse particles. Recently, the synthesis has been processed by mixing the reactants together, often by injecting one of chemicals into the remaining ones in a short time. This can make sure that the whole nucleation process in that short time, followed by a slower growth process, thereby attempting to separate the two stage temporally.

*3.2.2 Mechanism of Growth*

Nucleation occurs during some time with constant monomer concentration. The growth of particles surface start to occur which decrease the monomer supply. Nucleation ends when the concentration of monomer falls below the critical level for nucleation. Generally speaking, the surface to volume ratio in small particles is pretty high, the surface excess energy becomes very important in very small particles. For a solution which isn't in thermodynamic equilibrium, the formation of larger particles reduces the surface energy of the initial smaller particles, and this mechanism play an important role in the growth of nanocrystals. The monomers diffuse to the surface of nanocrystals and make bonding with surface atoms, and this process lets small particles become larger. Coarsening effects which controlled by mass transport or diffusion are often termed the Ostwald ripening process, and this diffusion limited Ostwald ripening process is the most important growth mechanism and was first quantified by Lifshitz and Slyozov[73], and the following related work was done by Wagner[74], known as the LSW theory.

The diffusion process is controlled by the surface energy of nanoparticles. The energy which associated with the difference between the chemical potential of atoms in an interfacial area and atoms in nearby bulk phase is called interfacial energy. In solid/liquid interface, with the chemical potential of particles increasing, the particles size decrease. The concentration of small particles in equilibrium solution is much higher than large particles, as described by the Gibbs-Thompson equation. The transportation of solution from small particles to large particles is led by concentration gradients. Depending on the local curvature of solid phase, the different curvature of equilibrium concentration of nanocrystals in the liquid phase set up concentration gradients and provide a driving force to grow the larger particles at the expense of smaller particles[75].

*3.2.3 Self-Assembly Growth of nanowires from Solution*[76]

It is still complicated to form nanowires from solution method. The growth of nanowires generally includes three steps: (1) crystalline seed formation; (2) Crystal growth by aggregation of monomers to seeds; and (3) surface stabilization by surfactants. So far, Scientists proposed several mechanisms for the anisotropy growth of nanocrystals in solution. The following are three typical mechanisms.

3.2.3.1 Solution-Liquid-Solid (SLS) Growth from Seeds

During the SLS reaction, the molecular precursor is decomposed at high temperature and generates monomers. In this kind of reaction, the metal catalysts are very small and easy to be activated at low temperature. The monomers react with the metal nanoseeds to form supersaturated alloy droplets (Figure 3.2). For example,

Semiconductor nanowires such like Si and Ge[77,78] grown from Au nanocatalyst under the supercritical fluid environment have been made. The ultra-thin nanowire[77] with 2-3 nm diameters have been fabricated by this method and the interesting optical properties have been observed .

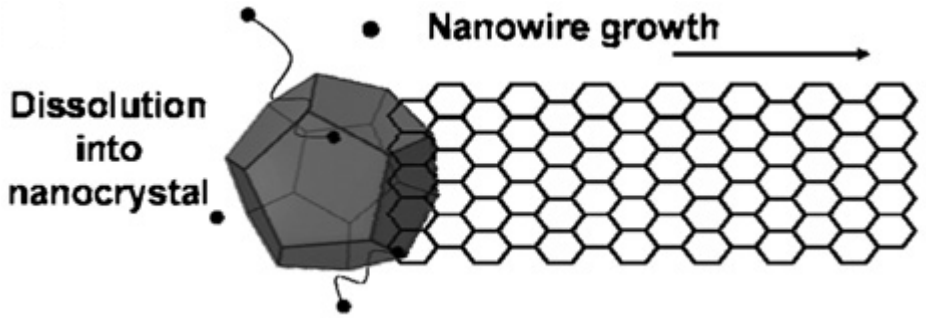


Figure 3.2 The growth of SLS process.

3.2.3.2 Self-Assembly Oriented Attachment Growth

The self-assembly attachment growth is based on the fact that nanoparticles generated in solution have a large surface-to-volume ratio. In order to reduce the surface energy and the total system energy, the nanoparticles may segregate together, and oriented attachment is one of the ways for this process. Penn and Banfield [79]observed this nanowires formation mechanism in the hydrolytic synthesis of $TiO_2$ nanocrystals. $TiO_2$ nanoparticles mainly included three face, {001}, {121} and {101}. The {001} has the highest energy and it is reasonable to remove this face since this is thermodynamic favorable. By this oriented attachment process, the nanoparticles are congregated along the [001] direction to remove the {001} face (Figure 3.3).

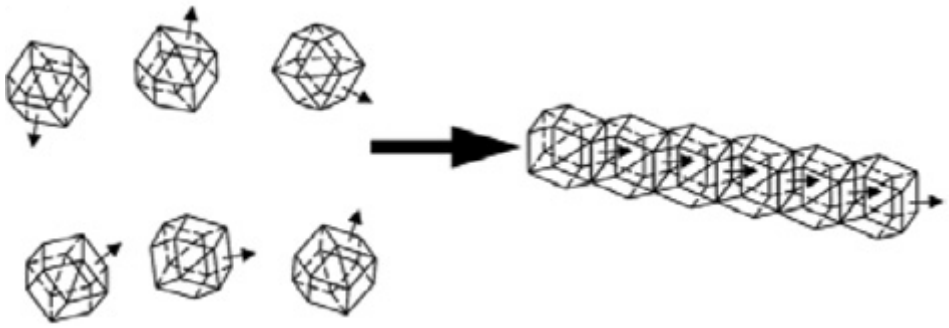

Figure 3.3 The Oriented attachment growth.

3.2.3.3 Anisotropic Growth of Crystals by Kinetic Control

Anisotropy growth caused by different surface energies is the mechanism for forming most elongated nanocrystals, but the difference of surface energies is not large enough to form highly anisotropy growth of nanowires. It is believed that the effective surface energy of nanocrystals can be modulated by adding surfactants to the reaction solution, and the surfactant molecules selectively absorb and bond on certain surfaces of the nanocrystal seeds. For example, the [001] is the first growth direction of $TiO_2$ nanocrystal in solution. By adding surfactants into reaction, the first growth direction can be changed to [101]. The role of surfactants is “structural directors”. This selective capping effect decreases the growth of these surfaces and increases the growth of nanocrystals in specific direction to form nanowires (Figure 3.4).

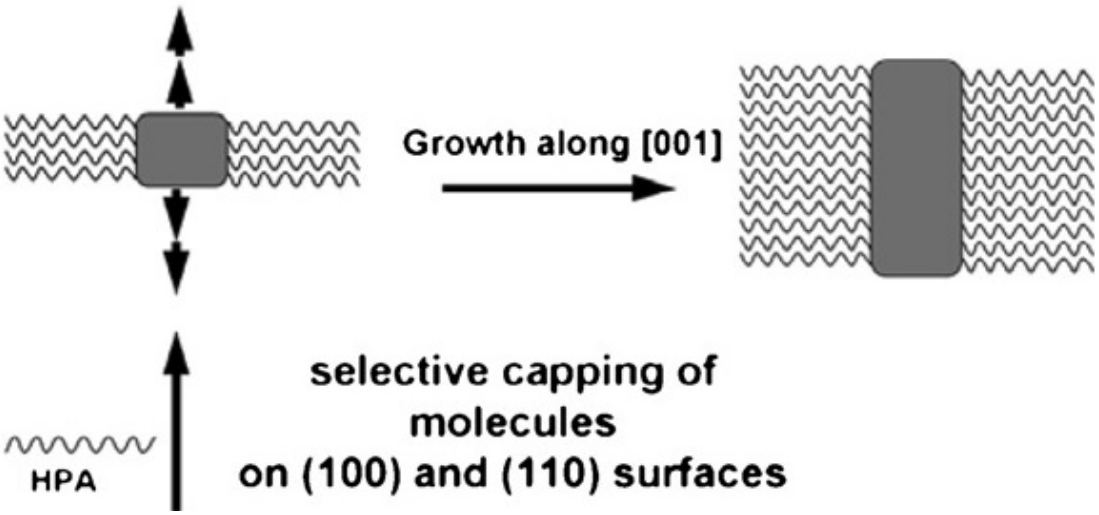


Figure 3.4 Surface selective surfactant assistant growth.

# CHAPTER 4

# CHARACTERIZATION FACILITIES

Transmission electron microscopy (TEM), high resolution TEM (HRTEM) and X-ray diffraction (XRD) were used for structural characterization. An Alternating gradient magnetometer (AGM) was used for magnetic characterization. A brief description of these equipments and characterization techniques and the techniques used to prepare samples are following.

## 4.1 X-Ray Diffraction (XRD)

Rigaku Ultima IV diffractometer with Cu-K $\alpha$ radiation (wavelength $\lambda$ =1.54056 nm) was used to characterize the crystalline structure of samples. The samples were prepared by drop casting dispersions of nanocrystals in solvents such as hexane or ether on the glass substrate. The sample was dried in the air and under a plastic cover to prevent the borne particles from the air. Samples were inserted into sample holder and analyzed between 20 – 90 $2\theta$ degrees. The incident X-ray follows Bragg's law as described in figure 4.1 and the following formula:

$$n\lambda = 2d \sin\theta \qquad (4.1)$$

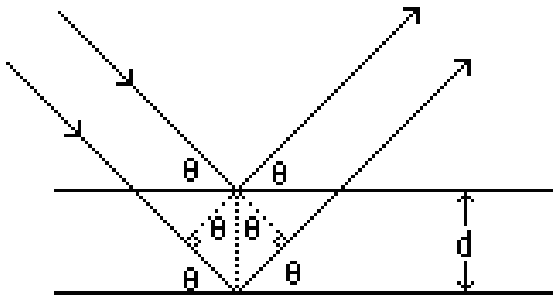


Figure 4.1 Bragg's law.

In an X-ray diffraction measurement, a monochromatic X-ray beam with wavelength $\lambda$ projected on a crystalline sample, and the sample gradually rotated to produce a diffraction pattern. The different d-spacing in the material are satisfied by Bragg's law, and the plotting of the angular positions and intensities show the characteristic of sample. Usually $2\theta$ is used instead of $\theta$.

For cubic crystals with lattice constant a, the spacing D between adjacent (hkl) lattice planes is:

$$D= a / (h^2+k^2+l^2)^{1/2} \qquad (4.2)$$

## 4.2 Alternating Gradient Magnetometer (AGM)

In AGM measurement, the sample is set on an extension rod attached to a piezoelectric element and placed it at the center of the poles that generates magnetic field. The sample is magnetized by a static DC field. An alternating gradient magnetic field is generated and produces an alternating force on the sample. This force (F) is

proportional to the magnitude of the alternating magnetic field (B) and the magnetic moment (M) of the sample.

$$F \propto B \,\&\, M \tag{4.3}$$

This force is converted into a proportional voltage by a piezoelectric element and hence the moment of the sample is measured. Samples with dimension up to 5 mm x 5 mm can be measured using AGM. The applied field is measured using a Hall probe sensor. The sensitivity of the AGM can reach up to 10 nemu. Due to availability only room-temperature measurements could be made using AGM. The maximum field that can be applied using AGM is limited to 14 kOe.

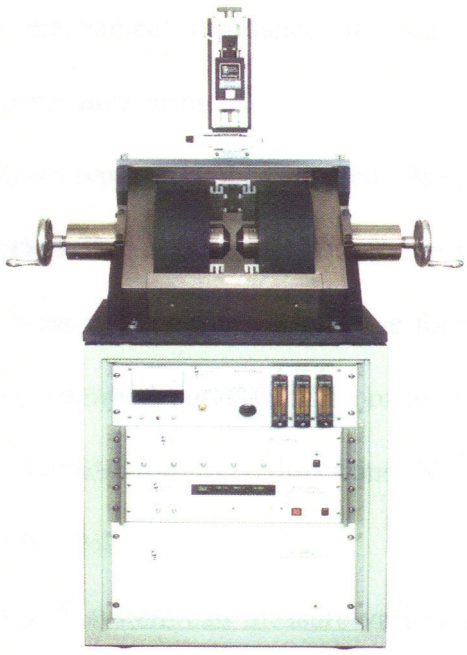

Figure 4.2 The Alternating Gradient Magnetometer (AGM).

## 4.3 Transmission Electron Microscope (TEM)

JEOL's 1200EX TEM was used for observing the crystalline structures and morphologies of nanocrystals. This TEM uses an acceleration voltage of 120 kV and can reach a magnification up to 500k times. The bright field images where the selected area electron diffraction (SAED) patterns were obtained on negative films, that were developed and scanned as digital images. Copper grids with carbon formvar backing were used for TEM samples. A drop of nanocrystals dispersed in hexane was put on the formvar side on TEM grid and the solvent was evaporated in air. It is very important to avoid the excessive surfactant on the particles surface, which reduces the contrast and quality of the images of nanocrystals.

The high voltage electrons generated from the filament are collected by the condenser lenses, then the electron beam transmits through the specimen, and project lens creates the images of specimen, and the projective lens project the image on the fluorescent screen. Magnification and focus can be adjusted separately by turning the objective lens and projective lens. Images can be recorded on the negative films by the camera placed on the bottom of the TEM. In the image mode, if the electron beam which transmits through the specimen is chosen to create image, then it is called bright field image. On the other hand, if the diffraction beam is chosen, it is called dark field image.

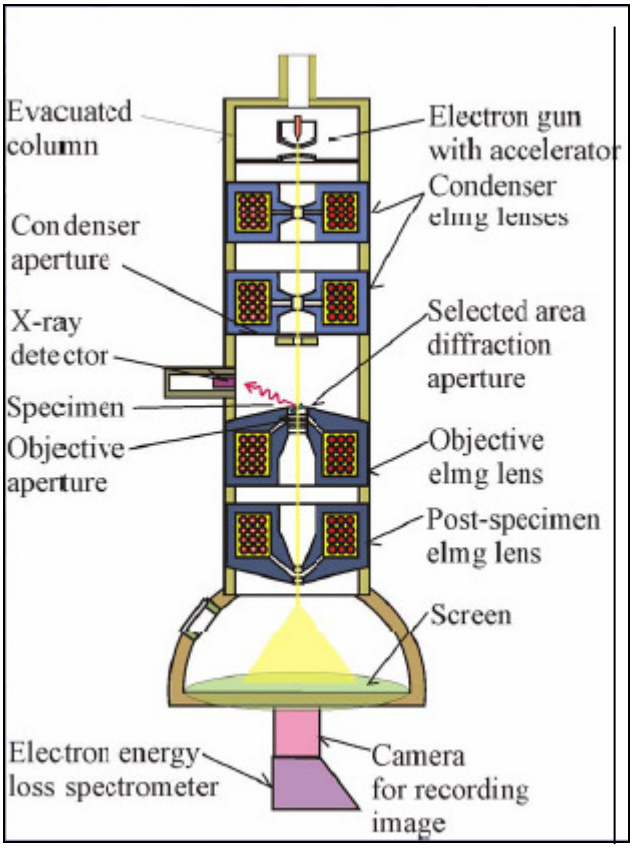


Figure 4.3 A typical structure of TEM.

High-resolution TEM images of selected samples were made by Hitachi HF 2000 TEM at Georgia Institute of Technology. The sample preparation for HRTEM analysis is the same to TEM.

# CHAPTER 5

# SYNTHESIS AND CHARACTERIZATION OF CoNi NANOWIRES

## 5.1 Introduction

CoNi nanowires have been extensively studied in the past years due to the great potential application in many areas include data storage and permanent magnets. Several techniques have been developed to fabricate CoNi nanowires, the most studies consist of the electrochemical deposition use porous polycarbonate membranes or anodic aluminium oxide as template[80]. However, Ung et al[81] made a progress on synthesis of high shape anisotropy CoNi nanowires by using solution phase method in 2006. In their research, high shape anisotropy nanowires can be obtained without template. The morphology of nanocrystals was controlled by varying parameters such as nanocrystals composition and the concentration of sodium hydroxide.

In this chapter, we report the chemical synthesis of cobalt and cobalt-nickel particles in sodium hydroxide solution of 1,2-butanediol with different shapes such as platelets, wires and particles. We reproduced the result of Ung's experiment, and tried other parameters such as catalyst and surfactant ratio to control the growth of CoNi nanocrystals.

The $Co_{80}Ni_{20}$ is the best composition to form isolated and elongated nanocrystals. In the same synthesis condition, pure cobalt particles are present a sea-urchin like shape, and the $Co_{50}Ni_{50}$ composition leads the formation of large

particles.The ratio of surfactants, pH level , and the amount of catalyst were varied to synthesize CoNi nanowires with tunable anisotropy, magnetization, and the dimension of both hard and soft magnetic material, which can further be used to fabricate devices for novel nanomagnetic applications.

## 5.2 Experimental

### *5.2.1 Synthesis of CoNi Nanowires*

#### 5.2.1.1 Synthesis in Flask

The synthetic experiments were performed under standard airless technique in nitrogen gas protection. For a typical procedure to prepare nanowires of 5 nm in diameter and 200 nm length, the mixture of 0.3253g cobalt(II) acetate tetrahydrate [$Co(ac)_2 \bullet 6H_2O$] and 0.0812g nickel(II) acetate tertahydrate [($Ni(ac)_2 \bullet 6H_2O$] and 10 mL of 1,2-butanediol was added to 125 mL flask with mechanical stirring. 0.0176g of $RuCl_3$ and 0.1237g of NaOH[0.15M] were added to two different glass vials, and 5 ml 1,2-butanediol was added to each vial and heated until all chemicals were dissolved. After purging the flask 20 min at room temperature, two solutions from vials were injected to flask, and the mixture was heated up to 100℃ for 30 min. The color of solution was changed to black during heating. When the precursors dissolved completely, then the mixture was continued heating to 180℃ in 10 min. 0.397 mL of TOP (Trioctylphosphine) and 0.282 mL of OA (Oleic Acid) were injected into flask in one minute after temperature was reached 180℃. The mixture was heated to reflux (180 ℃) for another 60 min under a blanket of Ar gas.

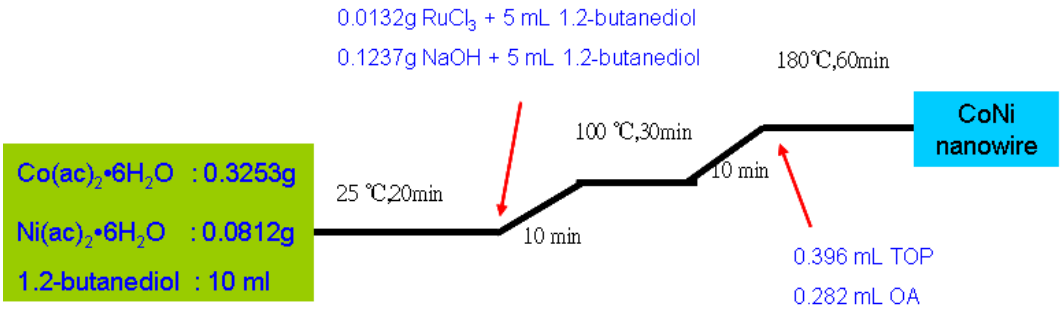


Figure 5.1 Schematic illustration of CoNi nanowires synthesis process.

5.2.1.2 Synthesis in Hydrothermal Reactor

All reagents are commercial products of analytically pure without further purification. In a typical procedure, 0.40 g cobalt acetate [$Co(ac)_2•6H_2O$], 0.12 g nickel acetate[ $Ni(ac)_2•6H_2O$], 0.43 g trioctylphosphine oxide (TOPO) and 0.28 mL were dissolved in 1,2-butanediol (BEG) (30 mL), the solution was constantly stirred for 30 min at room temperature under argon gas protection. Then the solution was heated to 100℃ and maintained in same temperature for 30 min for getting rid of water. Finally, the solution was obtained and transferred into a 50 mL stainless steel autoclave. The autoclave was sealed under argon gas protection and maintained at 180 ℃ for 2 h and then cooled down to room temperature naturally. The product was filtered off, washed with ethanol for several times, and finally dried in the air.

*5.2.2 Purification and Characterization of Co and CoNi Nanowires*

The black product which was precipitated in the flask can be removed to the tube by adding ethanol and separated by centrifugation. After washing the product in

ethonal three times, the solvent was removed and the product was dried in the air. For TEM sample preparation, a few drops of nanocrystals were well dispersed in hexane, and a drop of solution was put on the formvar side of TEM grid. The solvent was evaporated slowly in the air and nanocrystals were well dispersed on the grid. The samples for AGM measurement were prepared by fixing the powder with epoxy.

XRD was recorded on a Rigaku Ultima IV diffractionmeter with a Cu X-ray source. The magnetic hysteresis measurements were done with Alternating Gradient Magnetometer (AGM). The TEM images were recorded on JEOL 1200 EX electron microscopy at an accelerating voltage of 120 kV. HRTEM analysis was made at Georgia Institute of Technology.

## 5.3 Results and discussions

### *5.3.1 Morphology Control of CoNi Nanowires*

#### 5.3.1.1 Effect of pH Level

The NaOH plays a critical role in controlling the particle shape. After chemicals dissolved in the solution, the concentration of cobalt and nickel ions in solution was strongly depended on pH level. The concentration of metal cations affected the nucleation and the growing rate of nanoparticles (Figure 5.2). Cations were transformed into solid intermediate phase in basic solution. Due to this reason, as the reduction of metal cations happened in solution, increasing the basicity of the medium was equal to decreasing growing rate. The more amount NaOH adding into reaction, the lower cation concentration in the solution.

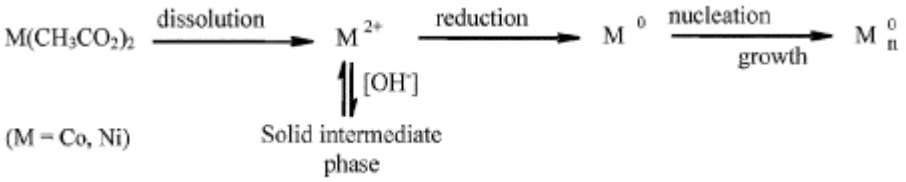


Figure 5.2 The illustration of Co and Ni growing process.

With increasing NaOH concentration, the particles, wires and plateles can be obtained. In $Co_{80}Ni_{20}$ nanocrystals synthesis, nanoparticles with 100 nm in diameter were formed without NaOH addition(figure 5.3a), and nanowires can be fabricated for [NaOH] varying between 0.10 and 0.18M(figure 5.3b). Further increase of the amount of NaOH to 0.21M leads to the formation of nanoplatets. (figure 5.3 (c)).

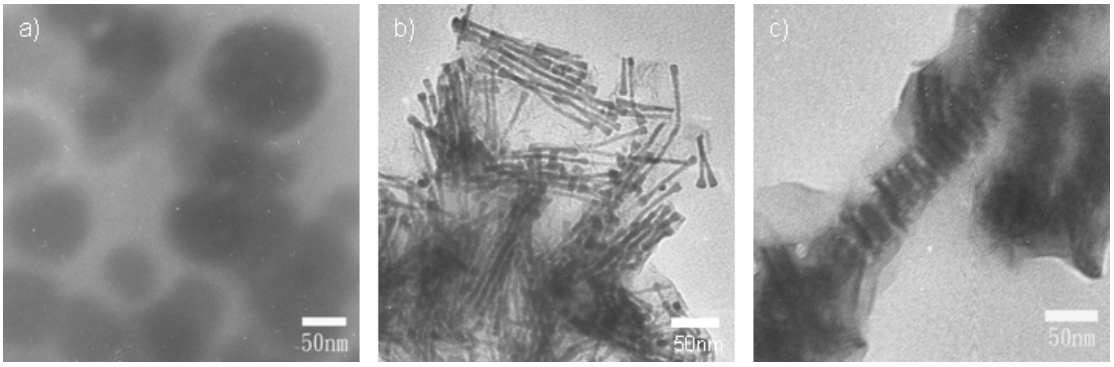


Figure 5.3 TEM images of $Co_{80}Ni_{20}$ nanocrystals in the shape of a) nanoparticles [NaOH] = 0M, b) nanowires [NaOH] = 0.15M, and c) nanoplateles [NaOH] = 0.21M.

The morphological and structural studies showed that the nanowires were the products of anisotropy growth along c-axis, which prefered the high growth rate[81]. It

can be concluded that the CoNi nanoparticles are formed with the higher growth rate that cause a non-controlled shape. The lower growth rate is better for controlling the shapes; the formation of nanowires need an intermediate growth rate due to platelets can be obtained with the lower one.

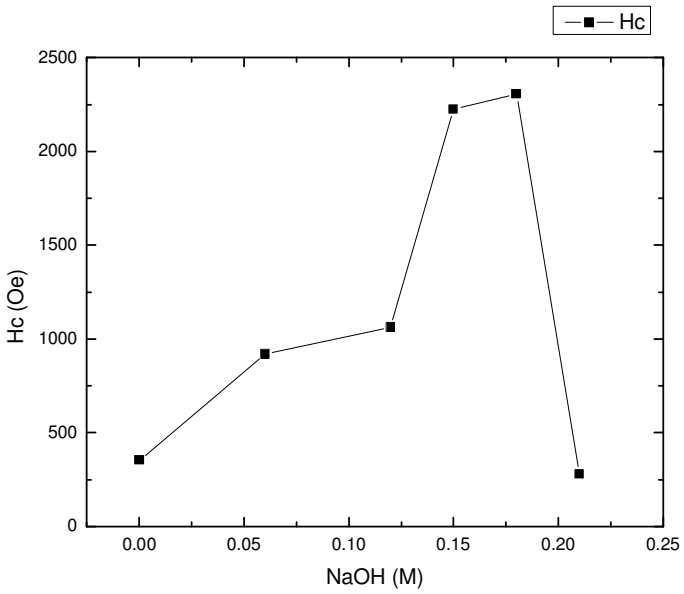


Figure 5.4 The relationship between the [NaOH] and coercivity.

In Figure 5.4, the coercivity increases with increasing amount of NaOH, but drops dramatically with the amount of [NaOH] exceeding 0.2 M. The growth rate of the hcp phase is strongly related to the crystallograohic orientation. Figure 5.5 shows the XRD pattern of $Co_{80}Ni_{20}$ synthesized with different NaOH concentration. The higher growth rate (lower NaOH concentration) favored to grow on (100) planes of hcp structure, lead to the shape of nanowire, whereas the lower growth rate (higher [NaOH])

favored to grow on (002) planes observed in platelets or particles. By comparing TEM and AGM results, we believe that the coercivity of CoNi nanowires was higher than nanoparticles, and the nanoplatelets got the lowest coercivity because the growing direction was paralleled to the easy axis.

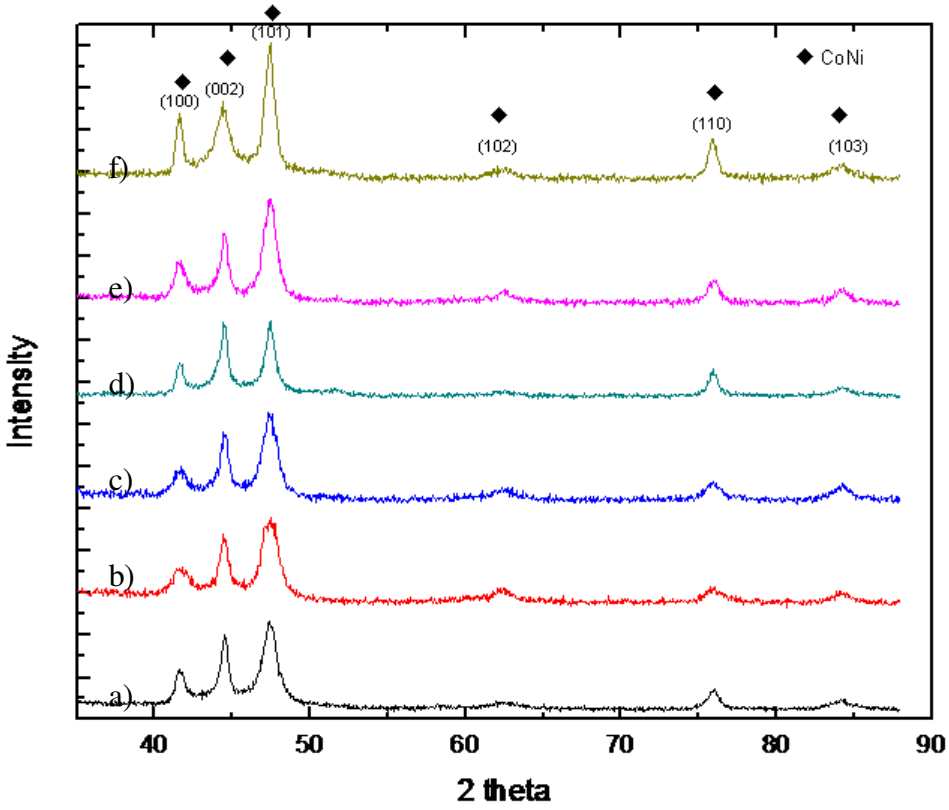


Figure 5.5 XRD patterns of CoNi nanocrystals synthesized with different [NaOH] a) 0 M, b) 0.06 M, c) 0.12 M, d) 0.15 M, e) 0.18 M, and f) 0.21 M

5.3.1.2 Effect of Catalyst

The catalyst particle attracts the target atoms with chemical potential in a certain distance. When the catalyst is supersaturated with atoms absorbed from the solution, atoms precipitate and form the alloy, causing the nucleation of the wire. With atoms continue to precipitate, a nanowire grow along the nanowire axis. As we discussed in chapter 3, the metal catalysts are easy to be activated at lower temperature. They lower down the requirement of nucleation and make reaction process much easier. If nanowires are grown on a catalyst which matches their lattice, the growth can be epitaxial.

The catalyst in this experiment was ruthenium, which is only known to present hcp structure even for a very small particle. Due to the same structure to cobalt, ruthenium becomes an ideal catalyst for the growth of $Co_{80}Ni_{20}$ nanocrystal. $RuCl_3$ decomposed after heating and generated the "seeds" for Co and Ni atoms bonding on the surface, then the seeds grew into CoNi nanocrystals. Varying the catalyst amount to metal salt ratio controlled the aspect ratio of the resulting nanowires. In Figure 5.6 (a), the agglomerated rods were obtained without catalyst. By adding 0.132g $RuCl_3$ into reaction, 50 nm long nanowires were produced. CoNi nanowires with 150 nm length and 5 nm in diameter have been synthesized with 0.176g $RuCl_3$.

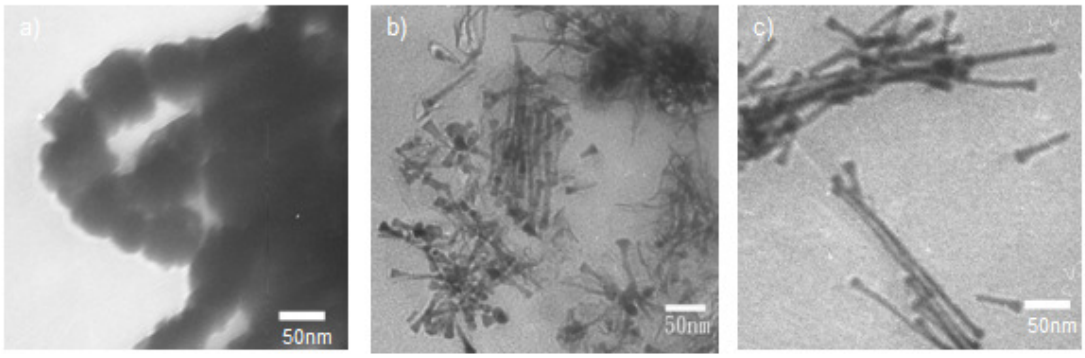


Figure 5.6 TEM images of CoNi particles prepared with $RuCl_3$ a) 0 g, b) 0.132 g, and c) 0.176 g.

Figure 5.7 shows XRD pattern of the CoNi nanocrystals synthesized by varifying catalyst amount. It was found that the product is a mixture of Co and Ni particles. By adding 0.066g of $RuCl_3$, the CoNi nanocrystals were obtained(figure 5.7 b). The higher anisotropy nanocrystals can be synthesized when more $RuCl_3$ added into reaction.

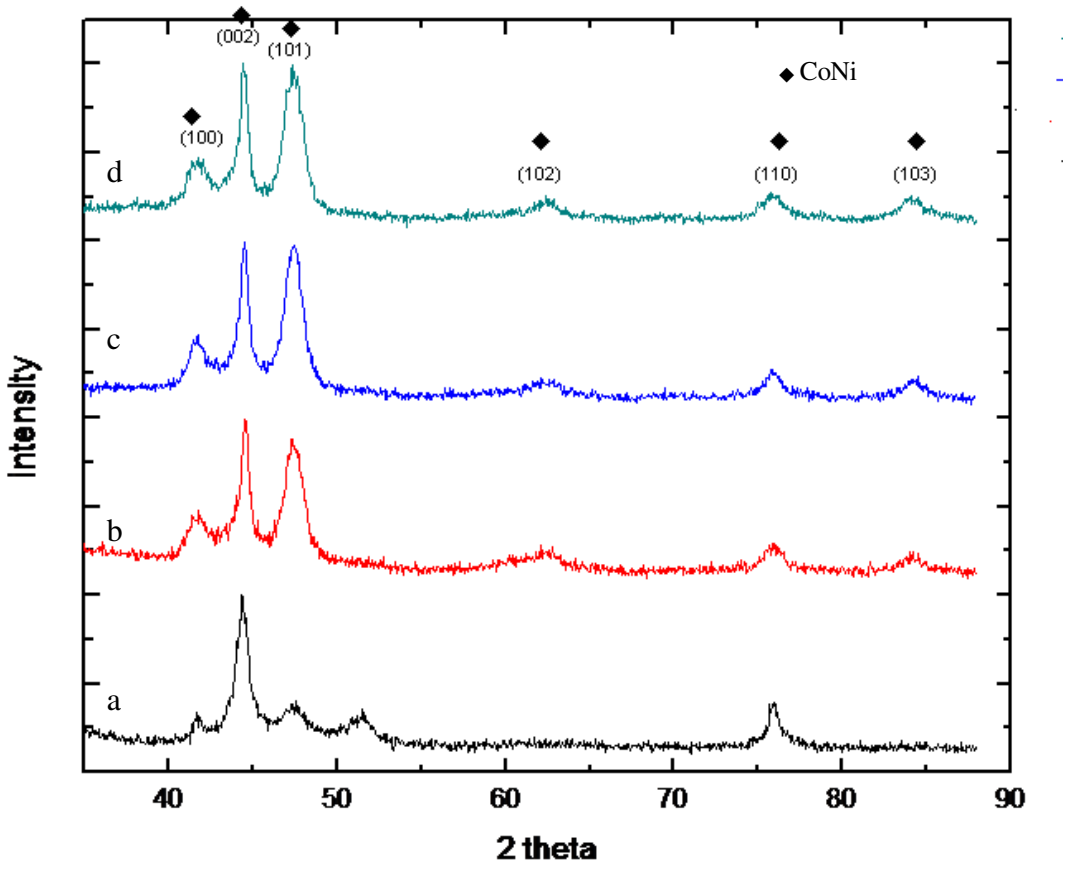


Figure 5.7 XRD patterns of CoNi nanocrystals prepared with different amount of $RuCl_3$ a) 0 g, b) 0.066 g, c) 0.132 g, and d) 0.176 g.

Comparing TEM and XRD results, the products of non-catalyst reaction were the mixture of particles with low anisotropy. Figure 5.8 showed that the coercivity of particles was low. After the addition of catalyst, nanowires were formed. The nanowires had higher coercivity than nanoparticles.

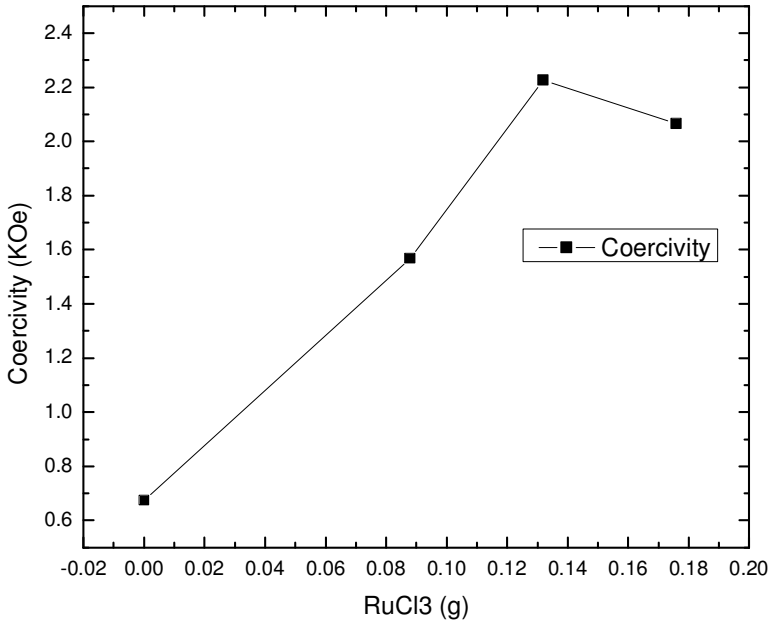


Figure 5.8 Dependence of coercivity on changing the amount of catalyst

5.3.1.3 Effect of Ratio between the Surfactants

The morphology of CoNi nanocrystals was mainly controlled by the chemical composition and the concentration of NaOH. Nanowires can be prepared in certain range of PH level, but surfactants still play an important role on controlling the length of nanowires. During the reaction, the surfactants were densely adsorbed onto the surface of the wires, forming a relatively close packed. By fixing pH level and varying the TOP/OA ratio, we found that the length of nanowires can be controlled. In Figure 5.9 (a), 75 nm nanowires can be formed with only oleic acid. With the increasing of TOP/OA ratio, nanowires became longer. The length of nanowires extended to 100 nm

when the TOP/OA ratio was 1:1. Figure 5.9 (c) shows 150 nm nanowires which were synthesized at 4:1 TOP/OA ratio.

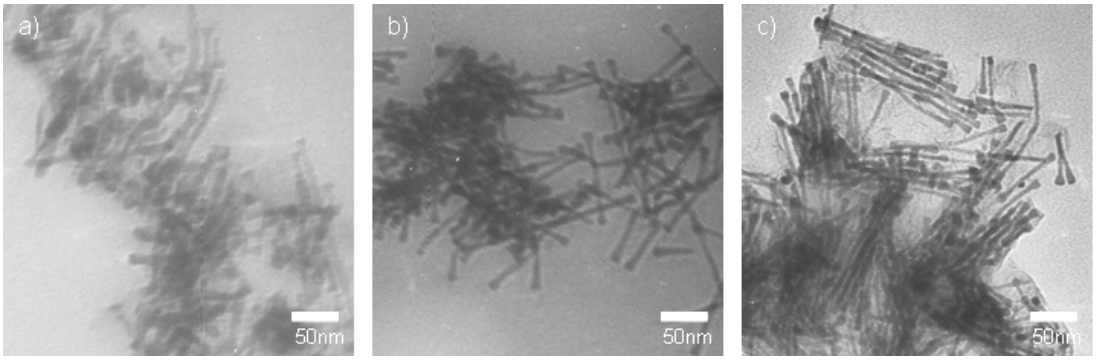


Figure 5.9 TEM images of CoNi nanocrystals prepared with different TOP/OA ratio a) 0:1, b) 1:1, and c) 4:1.

From Figure 5.10, The XRD pattern shows that the changing of TOP/OA ratio didn't affect the structure of CoNi nanowires. The coercivities were influenced by the interaction of CoNi nanocrystals and TOP.

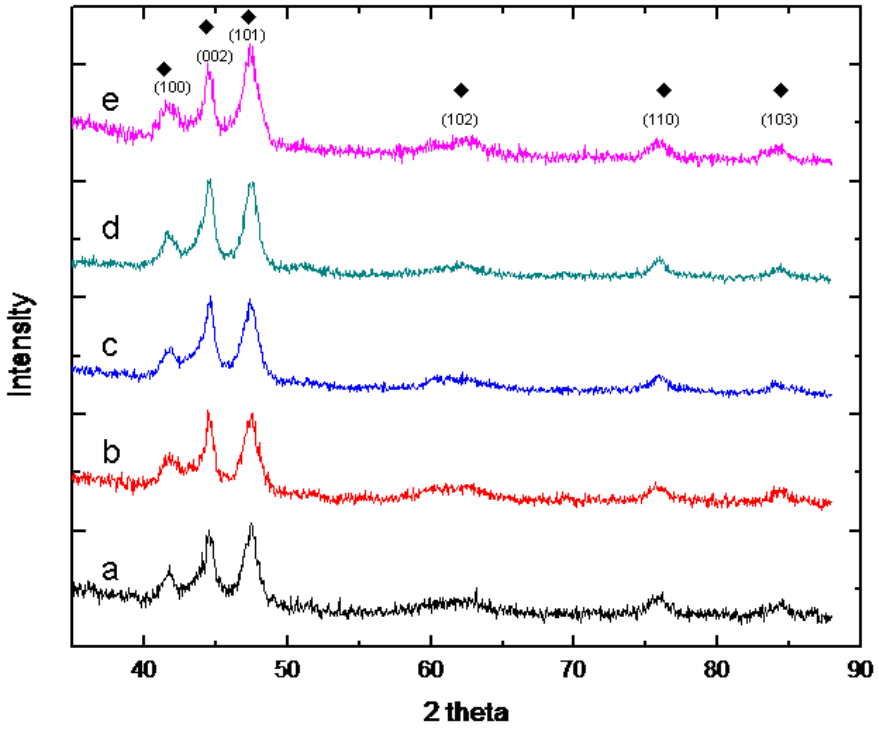


Figure 5.10 XRD patterns of CoNi prepared with different TOP/OA ratio a) 0:1, b) 0.5:1, c) 1:1, d) 2:1, and e) 4:1.

Figure 5.11 shows the coercivity dependence on verified ratio of TOP/OA. With increasing TOP amount, the coercivity became higher. The highest coercivity can be obtained when the TOP/OA ratio was 1:1. The coercivities decreased dramatically when the TOP was more than two times of OA. Although longer CoNi nanowires can be obtained with higher TOP/OA ratio, the coercivity was decreased when the TOP/OA ratio was more than 1:1. We believed that it may due to the interaction of CoNi nanocrystals and TOP that reduced the magnetic properties.

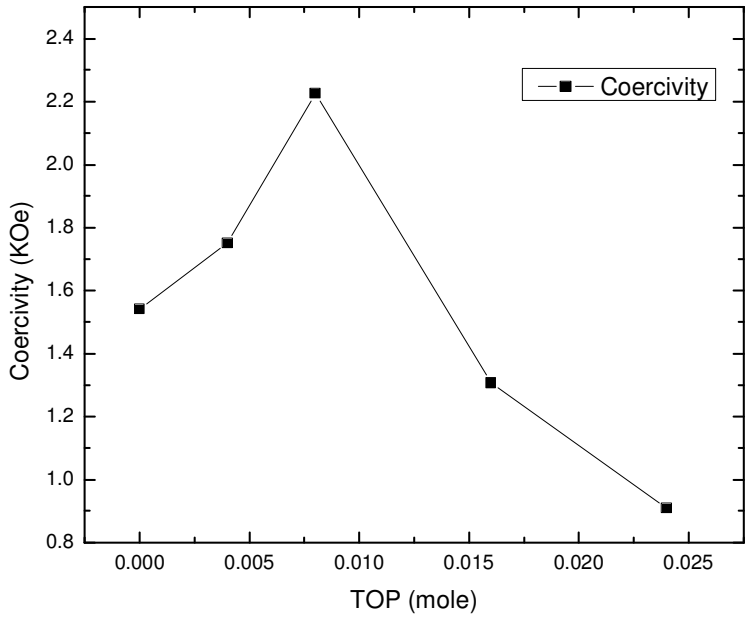


Figure 5.11 Variation in coercivity with changing the ratio of TOP/OA ( OA is remain 0.08ml).

*5.3.2 Structures and Magnetic Properties*

The structures of CoNi nanocrystals depend on the chemical composition. The cobalt nanowires prepared with [NaOH] = 1.6 M crystallize in the hcp structure, and the nickel particles prepared with [NaOH] = 1.5M with fcc one. The X-ray diffraction pattern of the $Co_{80}Ni_{20}$ nanowires shows mainly the hcp phase (figure 5.12). The peak of the [100] direction is broader than [002] direction. It means that the wires grew along the c-axis of hcp structure.

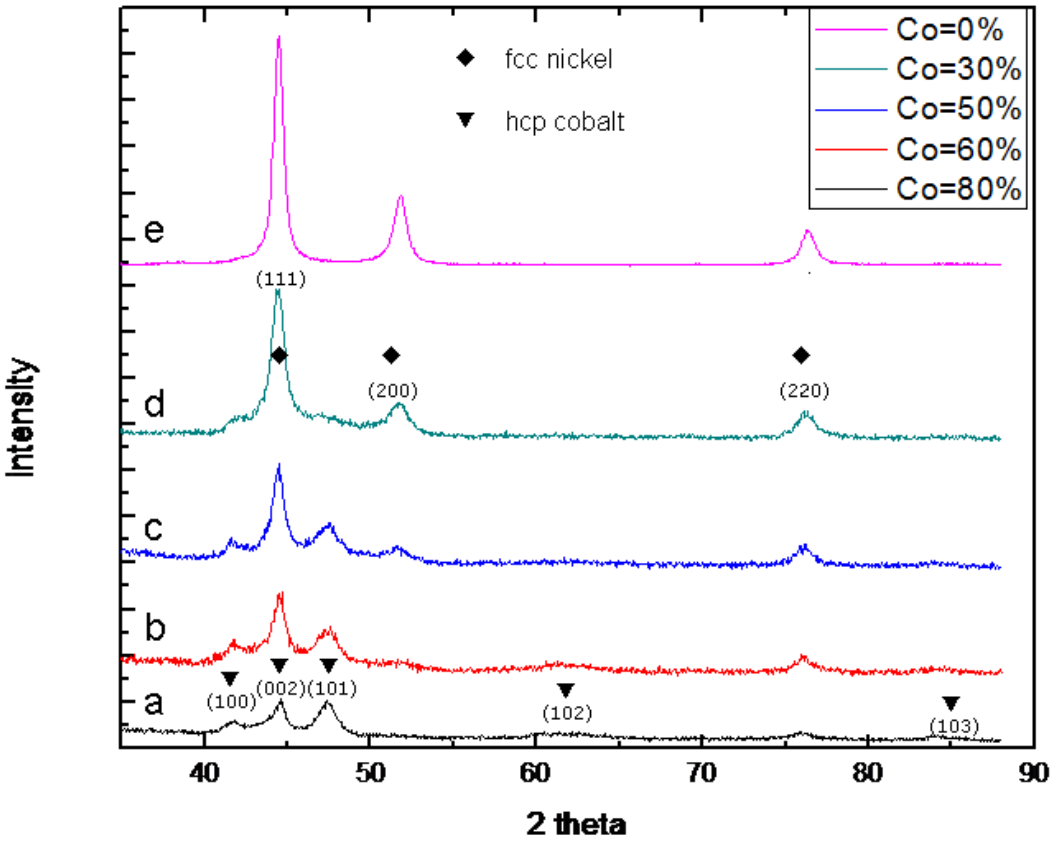


Figure 5.12 XRD patterns of CoNi nanocrystals a) $Co_{80}Ni_{20}$, b) $Co_{60}Ni_{40}$, c) $Co_{50}Ni_{50}$, d) $Co_{30}Ni_{70}$, and e) pure Ni.

The studies of morphology and structural showed that the wires are the products of the anisotropy growth along the c-axis of particle crystallizing with hcp structure. In this reason, wires can be obtained with high cobalt content. Figure 5.13 showed the TEM image of a) the pure Co nanocrystals with sea-urchin-like shape, but the CoNi nanocrystals with 20% nickel in composition showed the isolate-wire shape. The difference between the shape of pure cobalt and $Co_{80}Ni_{20}$ can be explained by the difference of growth rate. Pure cobalt nanocrystals can be obtained with a higher growth rate. For CoNi nanocrystals, the formation of nanowires can be explained by a

lower growth rate. In figure 5.13 c), TEM images showed that nanowires can be synthesized with the nickel lower than 40%. By increasing the content of nickel, due to the preference of growth direction of fcc structure[81], the nanocrystals attempt to grow perpendicular to c-axis, and thus the morphology of nanocrystals grew into the shape of particles and platelets. The growth rate should be constant in the same pH level. It is possible to conclude that the growth rate can be slow down with the addition of nickel.

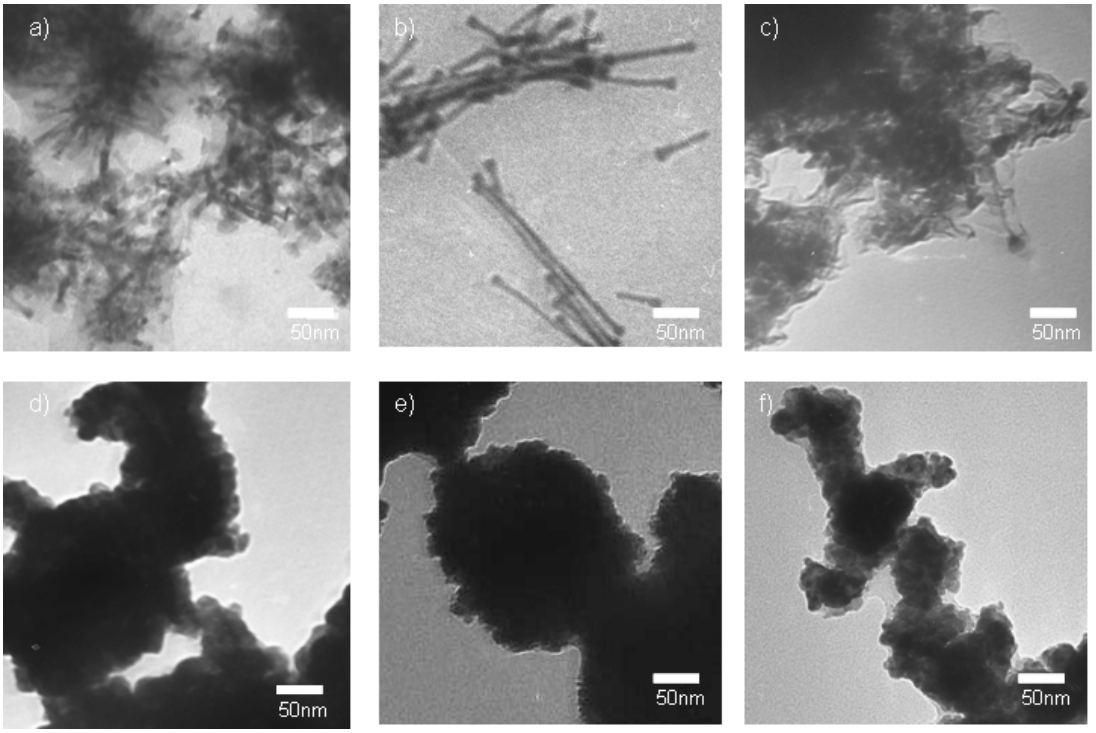


Figure 5.13 TEM images of CoNi with changing chemical composition
a) pure Co b) $Co_{80}Ni_{20}$ c) $Co_{60}Ni_{40}$ d) $Co_{50}Ni_{50}$ e) $Co_{30}Ni_{70}$ f) pure Ni

The CoNi nanocrystals are ferromagnetic materials at room temperature. The magnetization curve is related on the anisotropy. The coercivity decreased in the range 0.1 – 2.26 kOe when the content of nickel increased (figure 5.14).

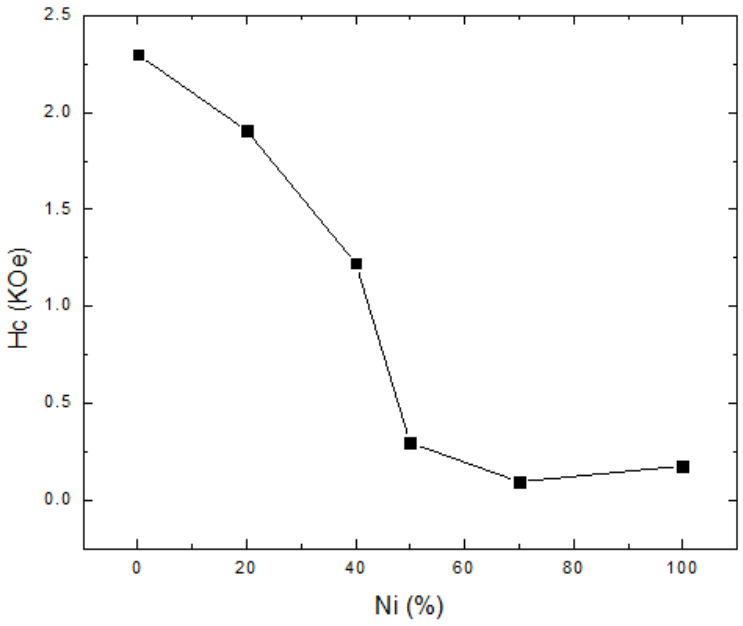


Figure 5.14 The coercivity changes with the different chemical composition of CoNi nanocrystals.

In figure 5.15 a), the HRTEM images showed the $Co_{80}Ni_{20}$ nanowires with 8nm in diameter. The column of nanowires crystallized with the hcp structure. The caps in the end of nanowire showed the fcc structure, which perpendicular to the c-axis (figure 5.15 c)). Comparing the XRD result, we believe that the caps of nanowires are nickel. It shows that the reduction rate of nickel is lower than that of cobalt.

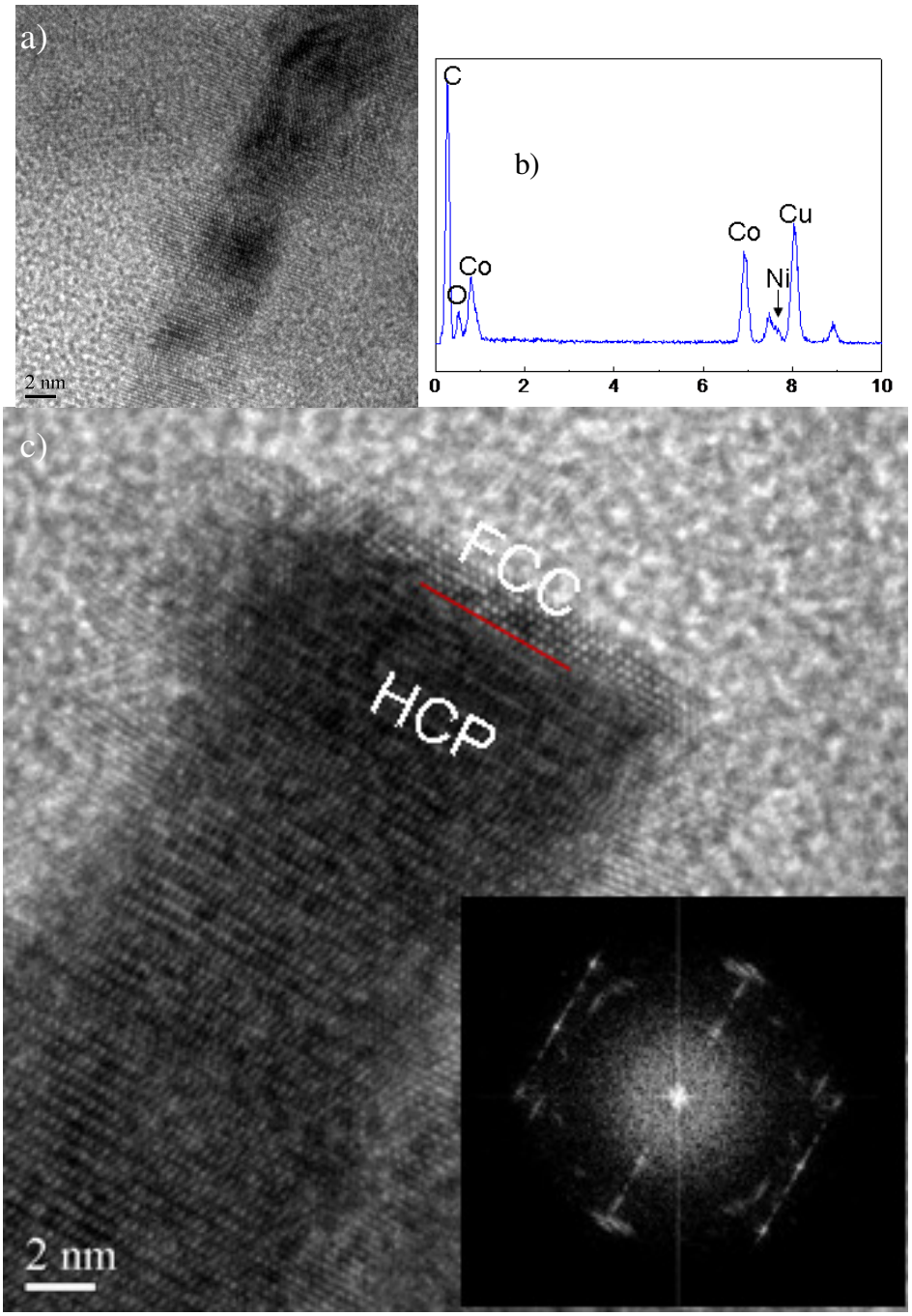


Figure 5.15 a) HRTEM images of $Co_{80}Ni_{20}$ nanowires with 8nm in diameter. b) EDX result of $Co_{80}Ni_{20}$ nanowires. C) HRTEM image of nanowires with hcp structure in the columns and fcc structures in the caps.

## 5.4 Conclusion

The shape of CoNi nanocrystals can be controlled by the growth rate, which is related to the NaOH concentration and cobalt-nickel composition. In the same synthesis condition, the sea-urchin-like shaped nanocrystals of pure cobalt can be obtained with high growth rate. Isolated CoNi nanowires can be fabricated with a slower growth rate by adding 20% Ni into composition. Either adding Ni or increasing the concentration of NaOH can slow down the growth rate, which favored (100) plane, and cause the growth in (200) plane, then leading the shape into platelets or sphere.

From the HRTEM image, it has been observed that the nickel is located at the end of nanowires. The main structure of the column of CoNi nanowires is hcp cobalt , showing that the reduction of cobalt is faster than that of nickel.

The length of nanowires can be controlled by varying the catalyst amount and the ratio between surfactants. By the selective absorb effect, surfactants can make temporary bonding on certain planes of nanocrystals, leading the anisotropy growth. The catalyst lowers down the requirement of nucleation. Cobalt and ruthenium have the same hcp structure, which made the growth become easier with the catalysis.

The highest coercivity of all the $Co_{80}Ni_{20}$ nanowires samples was 2.26 kOe, which was synthesized within 0.15M NaOH solution, the $RuCl_3$ was 0.176g, and the mixture of 0.008 mole OA and TOP in ratio 1:1. The nanowires with well control in morphology have 150nm in length and 5nm in diameter.

# CHAPTER 6

# SYNTHESIS AND CHARACTERIZATION OF CoFe NANOWIRES

## 6.1 Introduction

CoFe alloys have been studied widely in the past years due to their magnetic properties such as large permeability, high saturation magnetization, high Curie temperature and low coercivity. It can be used in advanced technical fields such as magnetic recorder, biomedical materials and electric vehicle generators. CoFe particles and films are not good magnetic recording materials due to their low magnetic anisotropy, but nanowire structure may have potential for magnetic data recording due to its size and morphology effect. The magnetic properties of the materials become strongly size dependent in nanometer size range. With weak crystalline anisotropy, magnetic properties may be mainly controlled by morphology, and nanowires can be used as high density data storage material (one bit per nanowire). Nanofabrication has been dramatically improved in past few years, and different groups have tried to produce $Fe_{(1-x)}Co_x$ nanowires in different method[82,83]. Most of them used templates such as anodic aluminum oxide (AAO) or metal step edges to synthesize CoFe nanowire alloys[82], or fabricate CoFe nanowire inside carbon nanotubes[83], but not many reports are about the CoFe nanowires synthesis in chemical solution. This chapter reports the chemical synthesis and characterization of CoFe nanowires. There are many reactionparameters that affect the particle size and shape of nanostructures during

chemical reaction. By controlling reaction parameters, different shape and magnetic properties of nanocrystals can be obtained. The condition to synthesize CoFe nanowires was found.

## 6.2 Experimental

### *6.2.1 Synthesis of CoFe Nanowires*

The synthetic experiments are under forming gas which is a mixture of 97% Ar +7% $H_2$. For a typical procedure to prepare nanowires of 2 nm in diameter and 90 nm length, 0.5 mmol of cobalt acetylacetonate, 0.75 mmol of iron acetylacetonate and 5 mmol 1,2-hexadecanediol was added to 125 mL flask containing a magnetic stir bar and mixed with 1.2 mL of oleic acid (OA). After purging 20 min at room temperature when the oxygen in the flask was almost removed, 2.28 mL trioctylphosphine (TOP) was added using a syringe, and flask was heating up to 100℃ for 10 min. The color of solution was changed from light pink to black during heating. The flask was continued heating to 200℃ for 10 min and kept to this temperature for 30 min, then it was heated to 300℃ for 10 min and kept at this temperature for 90 min. Forming gas was flowed throughout the experiments. The heating rate was varied from 2℃ to 15℃ per minute according to experiment design.

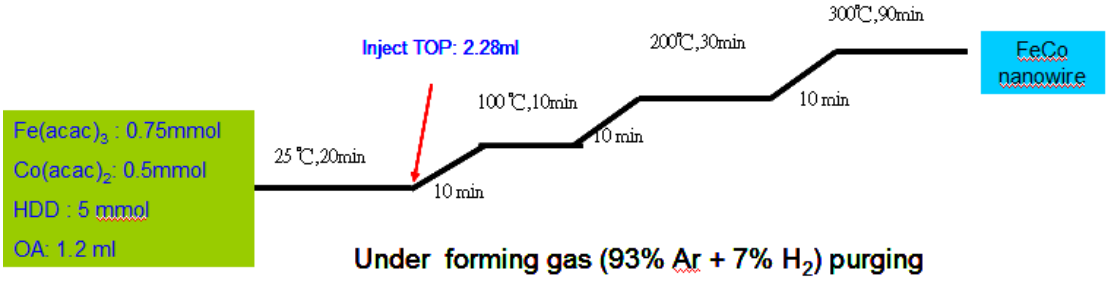


Figure 6.1 Schematic illustration of CoFe nanowires synthesis process.

To control morphology, several parameters that may affect the size and shape of CoFe nanocrystals were examined. It was found out that the concentration of solution, the ratio between surfactants, amount of reducing agent and the heating rate between 200℃ to 300℃ are the key parameters in size and shape control of the CoFe nanocrystals.

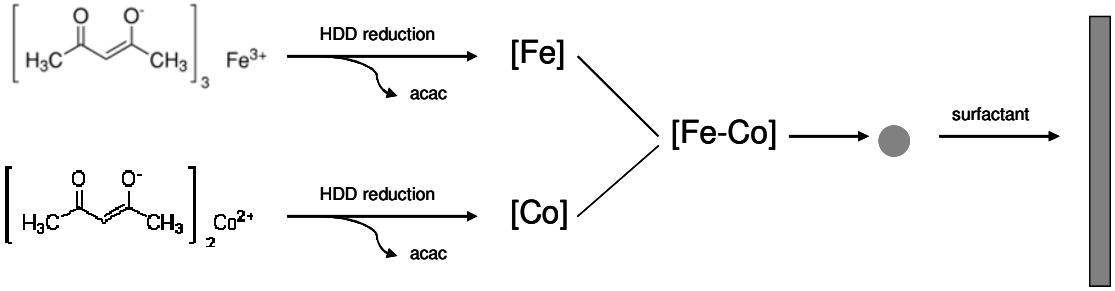


Figure 6.2 Schematic illustration of CoFe nanowires forming from the reduction of $Fe(acac)_3$ and $Co(acac)_2$.

*6.2.2 Purification and Characterization of CoFe Nanowires*

CoFe nanostructures are very sensitive to oxygen. To prevent from oxidation and also for better soluability, 20 ml hexane was added into flask before product was

removed. After washing the products in ethanol by sonication and centrifugation for three times, the particles were dispersed in hexane and stored in the plastic tube.

The CoFe nanocrystals were found to be slowly oxidized when exposed to air, forming an oxide shell and decreased $M_s$. In order to obtain the accurate data, all of the XRD and AGM measurements were made within 2 hrs of nanocrystals synthesis. To prepare AGM samples, a drop of nanocrystals solution was put on a piece of paper and wait until it dries, after measuring the weight with microbalance, then covered by a drop of epoxy and wait for 30 min to dry. To prepare TEM samples, a drop of nanocrystals dispersion solution in hexane was put on a 300-mesh carbon coated cooper TEM grid. The solvent was evaporated slowly in the air and nanocrystals were well dispersed on the grid.

XRD was recorded on a Rigaku Ultima IV diffractionmeter with a Cu X-ray source. The magnetic hysteresis measurements had been done with AGM. The TEM images were recorded on JEOL 1200 EX electron microscopy at an accelerating voltage of 120 kV. HRTEM analysis was made at Georgia Institute of Technology.

## 6.3 Results and discussions

### *6.3.1 Effect of Solvent*

Solvents are the media for particles to nucleate and grow. The certain composition of Fe and Co is required to form the desired phase. Due to the synthesis requirement of high temperature, CoFe nanocrystals are formed in the proper solvent with high boiling point and chemical stability. Oleic acid (OA) is an ideal solvent for

our experiments due to the high boiling point which is 360℃, and its stability at reflux temperature (300℃). The excellent solubility to precursors is also an important reason to select OA as the solvent. Oleylamine had been used as a solvent in this experiment, and the experiment was failure because the high viscosity of the solvent and precursors did not dissolve in the solvent.

The size and shape of nanocrystals can be controlled by changing the amount of solvents. TEM image showed that 50nm long nanowires could be fabricated with 1.2ml OA (figure 6.3 b), and the $M_S$ was 91.25emu/g (figure 6.4). By adding more OA, the products became a mixture of nanorods and nanoparticles(figure 6.3 c). Nanowires disappeared after OA amount higher than 1.5ml, and the formation of nanoparticles lead to the decreasing of saturation magnetization. The experiment result indicated that the saturation magnetization of CoFe nanocrystals can be varied by controlling the morphology. Nanocrystals with wire or rod shapes had higher $M_S$, whereas the one with particle shape came with lower $M_S$.

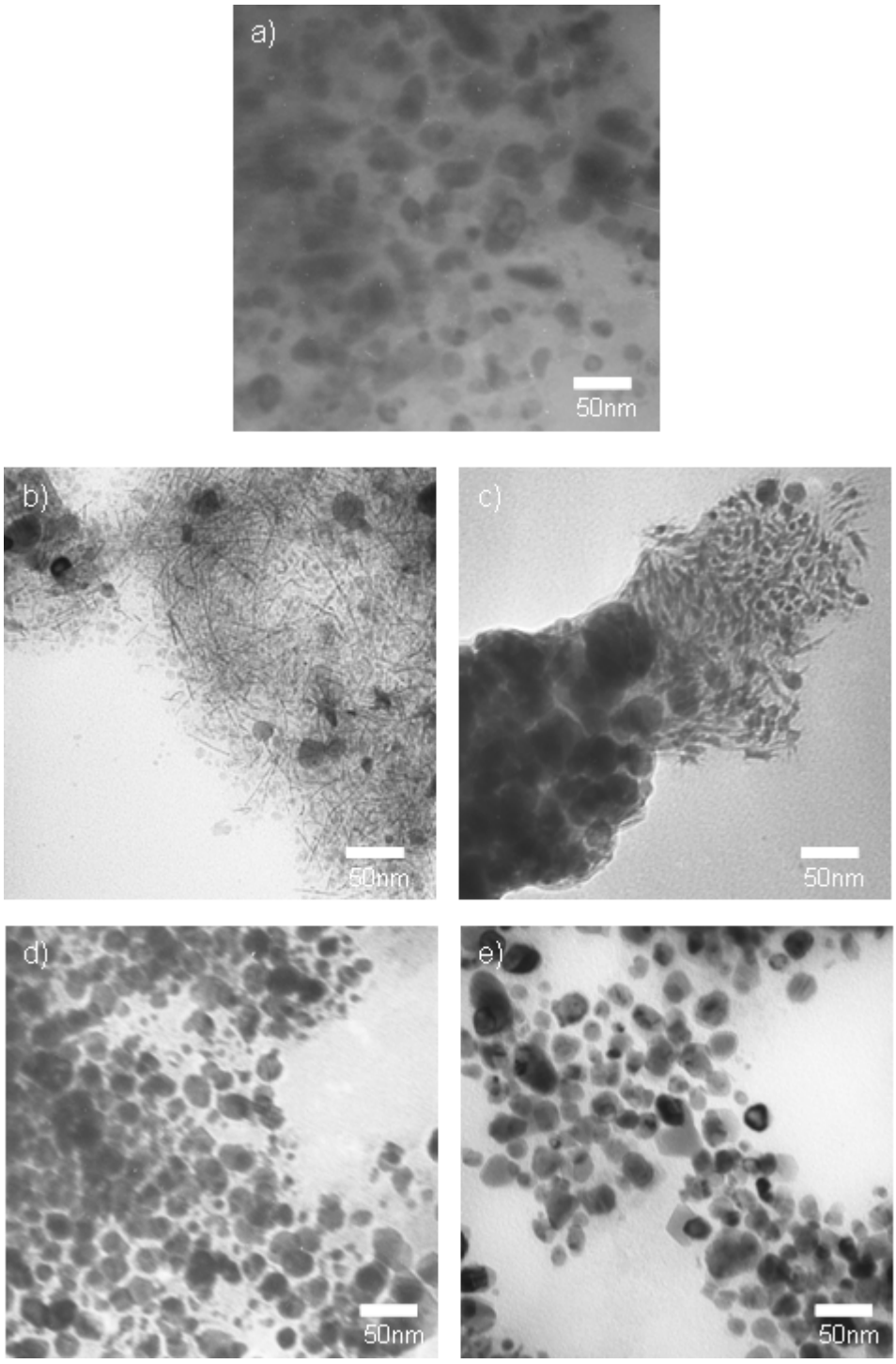


Figure 6.3 TEM images of CoFe with varying OA amount a) 1.0 ml, b)1.2 ml, c)1.4 ml, d)1.6 ml, and e)1.8 ml.

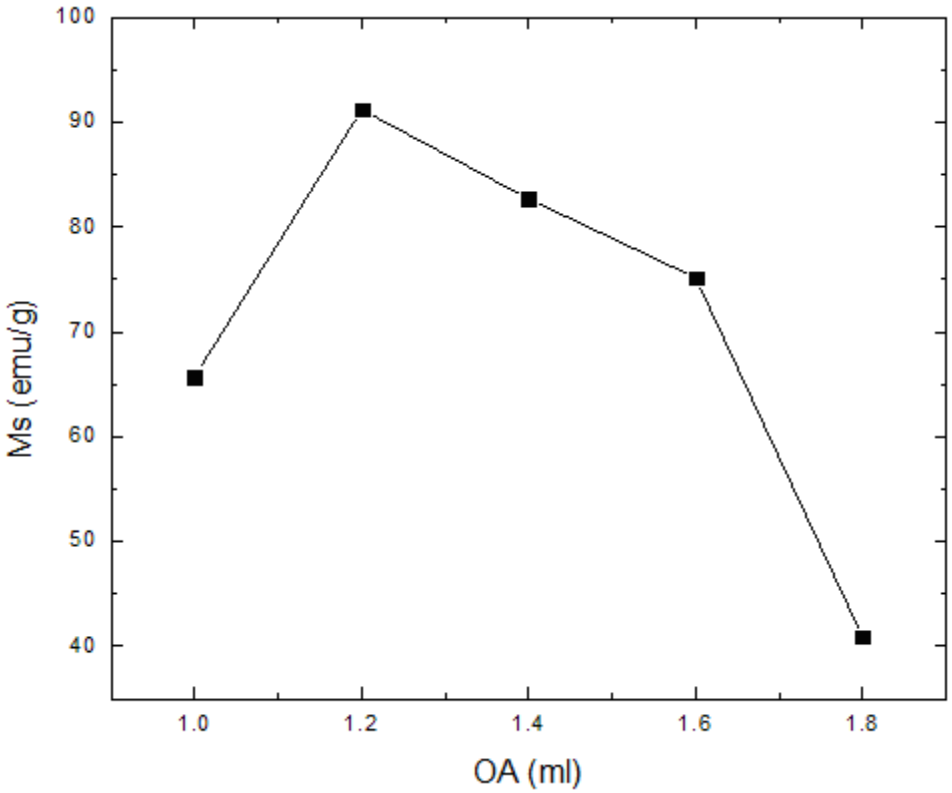


Figure 6.4 The saturation magnetization change of CoFe nanocrystals with varying OA amount.

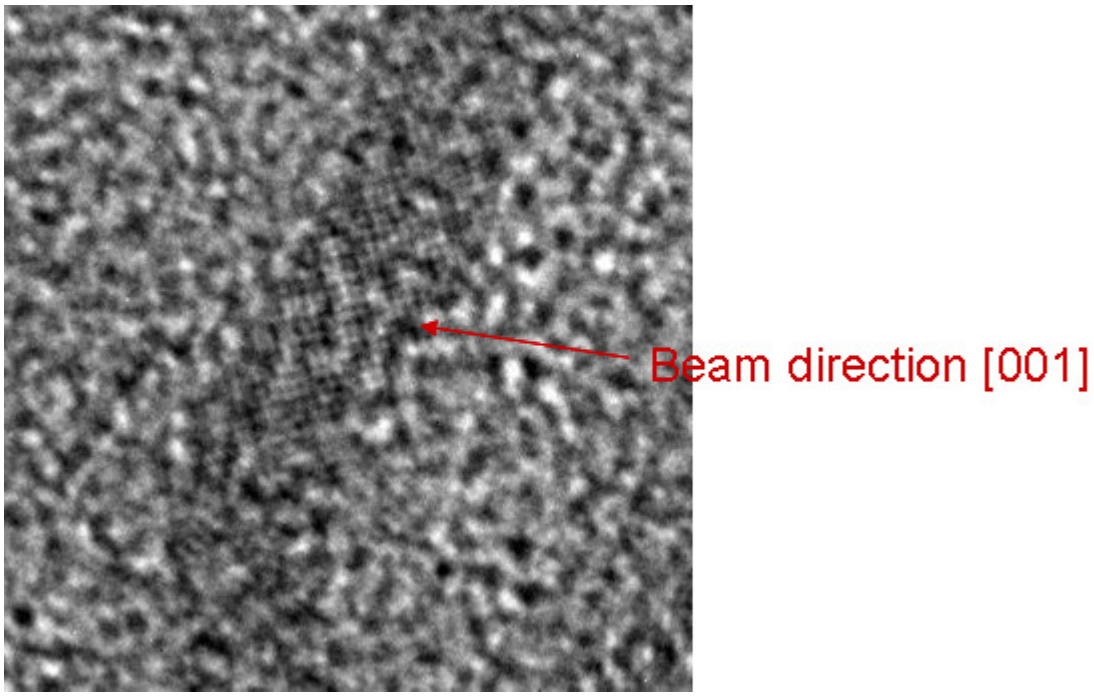


Figure 6.5 HRTEM image of CoFe nanowires with beam direction [001].

Figure 6.5 showed the HRTEM of CoFe nanowires image, which was taken with [001] beam direction. Compared with CoFe XRD pattern (figure 6.6 ), we believe that the orientation of CoFe nanowires may be (200) or (110) direction.

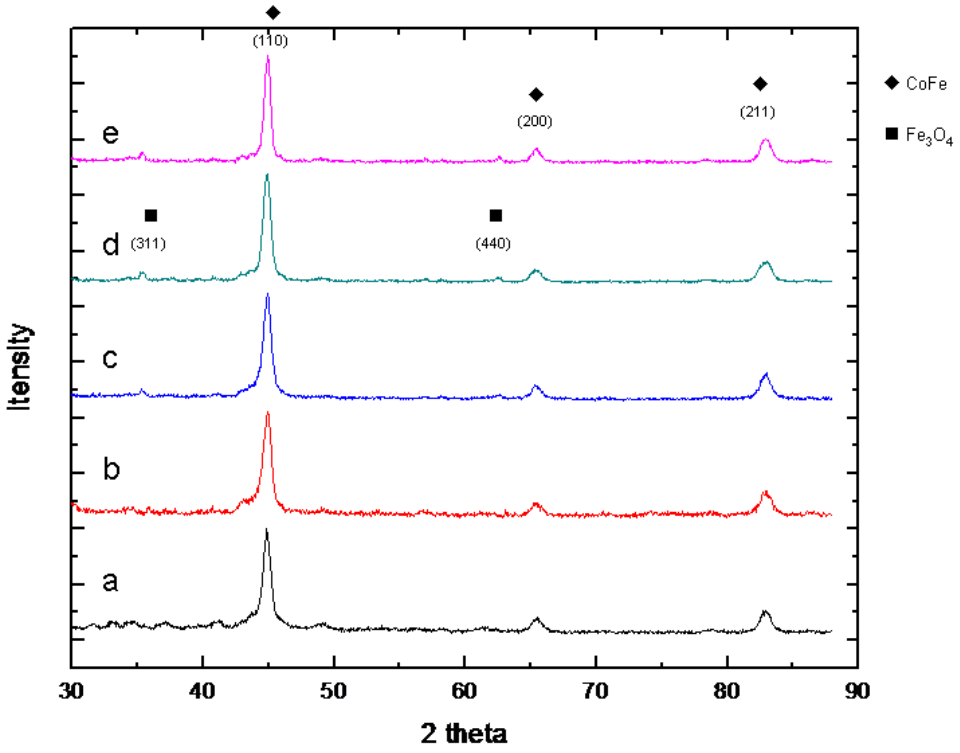


Figure 6.6 XRD patterns of CoFe with changing OA amount a) 1.0 ml, b) 1.2 ml,c) 1.4 ml, d) 1.6 ml, and e) 1.8 ml.

*6.3.2 Effect of Surfactants Ratio*

In past few years, surfactants-assistant method has been broadly applied on nanocrystals fabrication. Surfactants play a critical role to control size and shape during chemical synthesis. The interaction between metal atoms and surfactants can be identified as coordination bonding. The function groups donate the lone-pair electrons to the empty d orbitals of the metal atoms and make a bonding. In this experiment, TOP (trioctylphosphine) and OA are surfactants with –P and –COOH function groups.

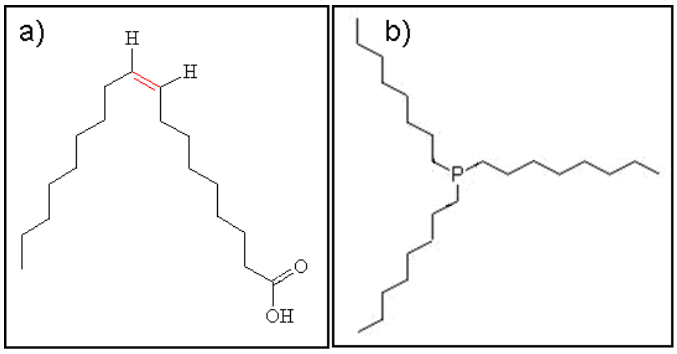


Figure 6.7 Molecular structures of surfactants a) OA and b) TOP

The size and geometric structures of these surfactants are also very different. OA has a single long alkyl chain ($C_{18}H_{33}$) with carbon double bond at the ninth carbon, and TOP has three shorter hydrocarbon chains ($C_8H_{17}$). These differences of structures cause that surfactants have different reactivities, and this phenomenon is called steric effect.

The lowest bonding energy of metal-surfactant coordination bond is related to the surface energy of materials and electronegativity of function group. Different surfactants have their favorable bonding-face, and the strength of bonding is also different. The coordination bonds between metals and TOP are easy to break due to the bulky chains of TOP preventing them packing tightly on the surface. During the reaction, the faces with OA bonding on the surface were well covered and can not grow anymore, but the faces which had coordination bonds with TOP were not stable and the bonding was easy to break, and the nanocrystals could be expanded by growing with free metal atoms.

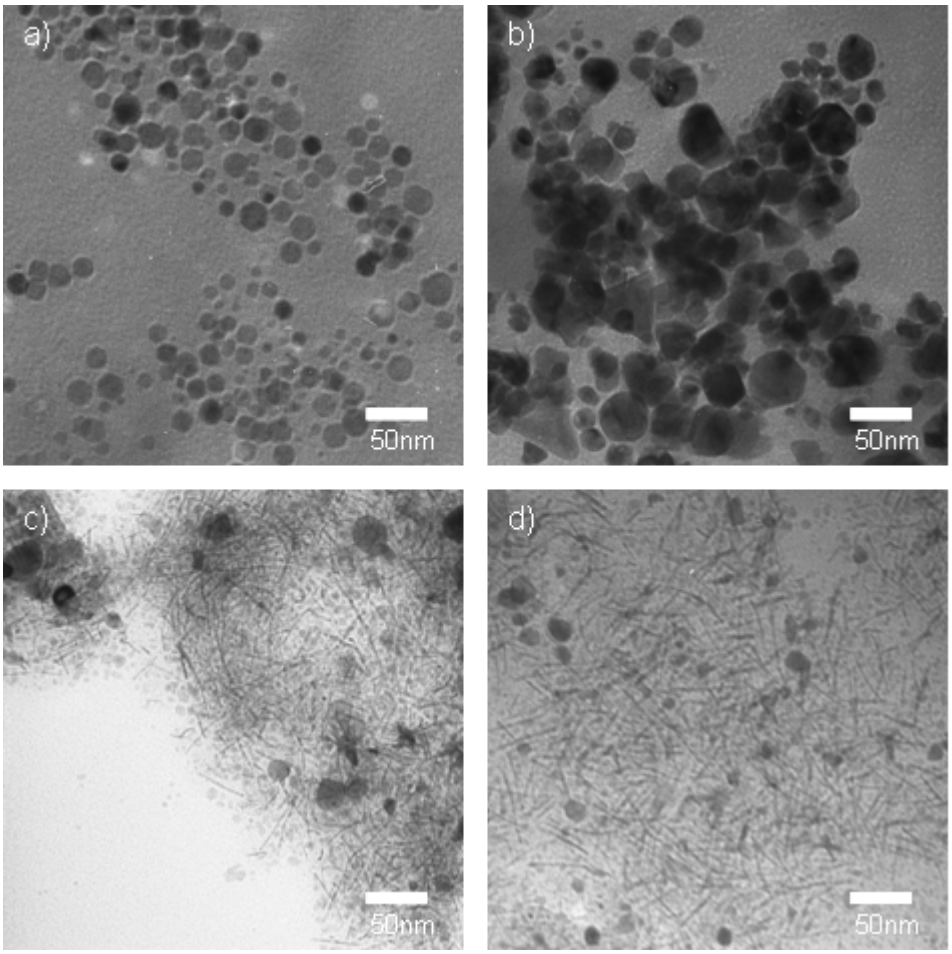


Figure 6.8 TEM images of CoFe nanocrystals synthesized with different TOP amount(a) 0 mL, (b) 1.14 mL, (c) 2.28 mL, and (d) 3.42 mL.

Figure 6.8 shows that the nanowires can not be formed without adding TOP, and the particle size was growing further after addition of more TOP into reaction. Nanowires were obtained at a certain TOP/OA ratio was used, but the concentration of solution decreased with too much TOP added, and the yield and the length of nanowires were also decreased.

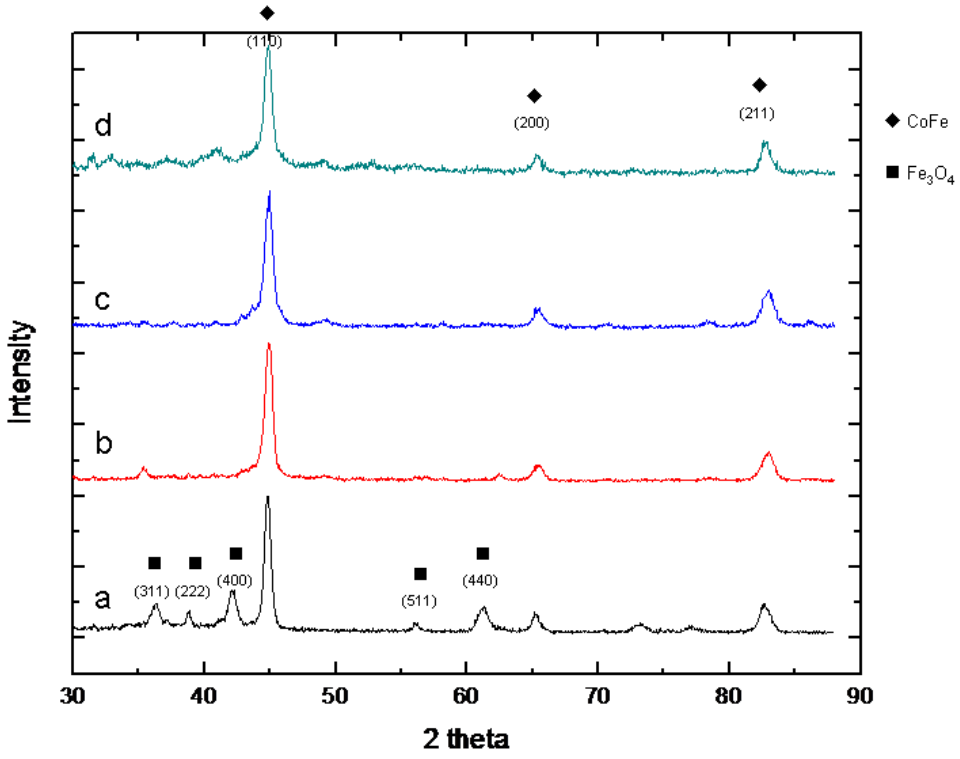


Figure 6.9 The XRD patterns of CoFe nanocrystals synthesized with different TOP amount (a) 0 mL, (b) 1.14 mL, (c) 2.28 mL, and (d) 3.42 mL.

The XRD patterns show that the oxidization occurred in the reaction without addition of TOP (figure 6.9). TOP is very reactive to oxygen, and it may consume the oxygen molecules in the solution to prevent the oxidation of metal atoms. The saturation magnetization were increased with more TOP in the solution, but drop dramatically when TOP was more than 2.5 ml (figure 6.10). Because TOP was hard to remove from the surface of nanocrystals, we believed that with adding to much TOP, the weight of CoFe nanocrystals increased, then decrease the saturation (emu/g).

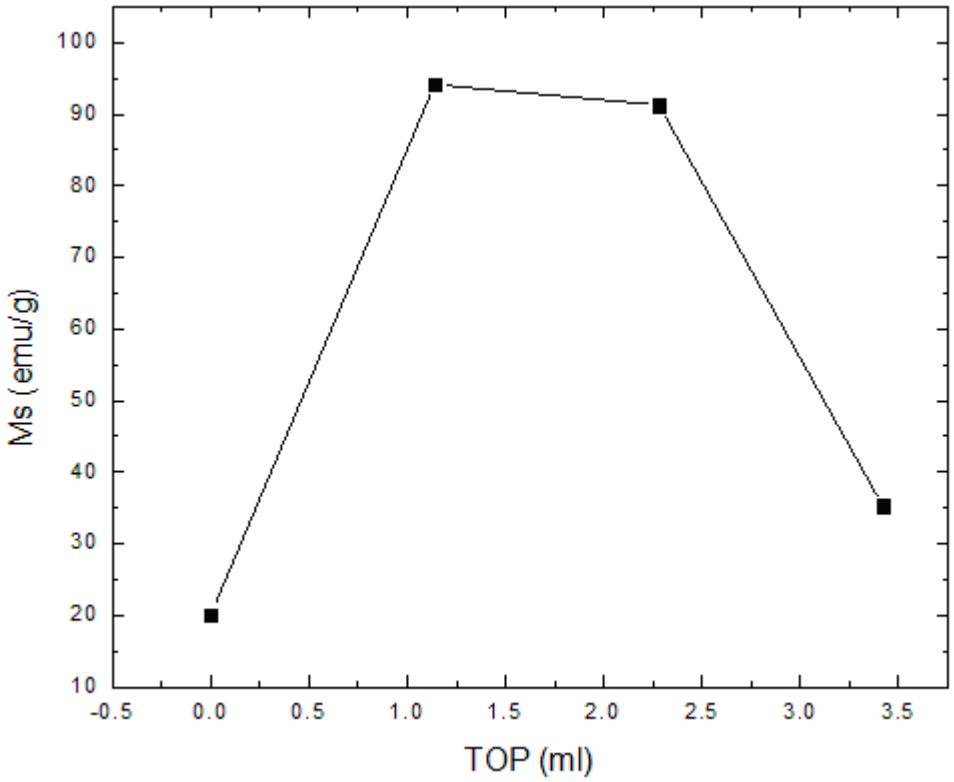


Figure 6.10 The changing of saturation magnetization with amount of TOP.

*6.3.3 Effect of the Reducing Agent*

Magnetic metallic nanocrystals can be prepared from metal salts using strong reducing agents. In this experiment, 1,2-hexadecanediol (HDD) was used as a reducing agent and reduced $Fe^{3+}$ and $Co^{2+}$ to Fe and Co atoms. There were two hydroxyl (—OH) groups separately bounding on the last two carbons of HDD (Figure 6.11).

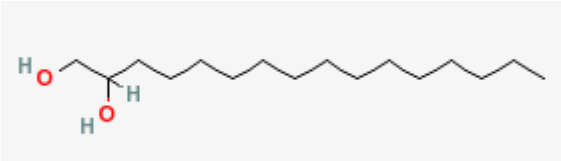


Figure 6.11 Molecular structure of HDD

During the reaction, oxidation of these two hydroxyl groups formed a ketone and an aldehyde, and the aldehyde was easily oxidized further to give a carboxylic acid(Figure 6.12). Due to the oxidization of HDD, $Fe(acac)_3$ and $Co(acac)_2$ were reduced to Fe and Co atoms and formed the nanocrystals

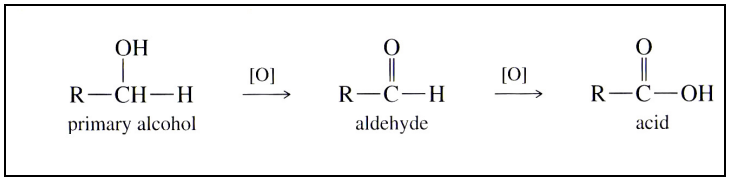


Figure 6.12 The oxidization process of hydroxyl group.

The reducing rate was owing to the difference between the reduction potential of $Fe^{3+}$ and $Co^{2+}$, and the HDD oxidation ability. By controlling HDD amount, Fe and Co atoms can be reduced at the same time. Metal atoms assembled together and formed nanocrystals. At the fixed ratio of precursors, the yield of nanowires can be controlled by adding the proper amount of HDD.

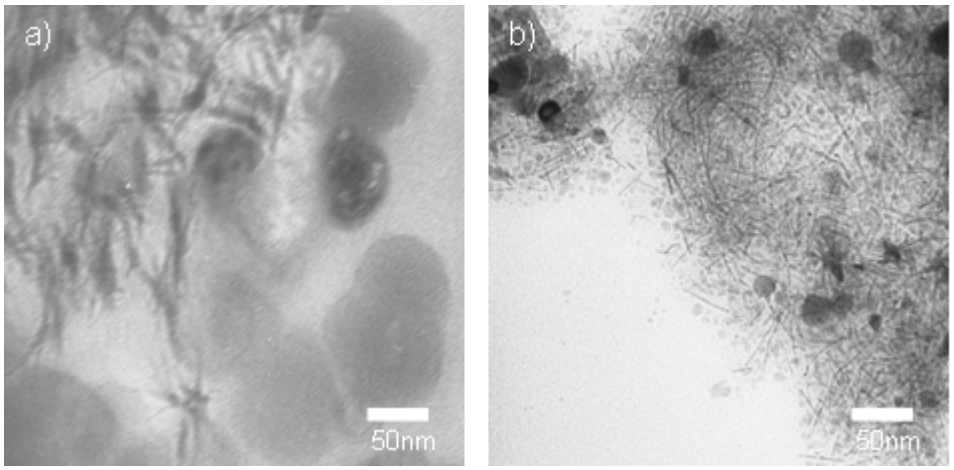


Figure 6.13 TEM images of CoFe nanocrystals synthesized with different HDD amount a) 0 mmole and b) 5 mmole.

In figure 6.13(a), nanowires can be formed without adding HDD due to the reducing ability of forming gas, but most of products were large nanoparticles. By adding HDD in proper amount, high yield of nanowires can be obtained.

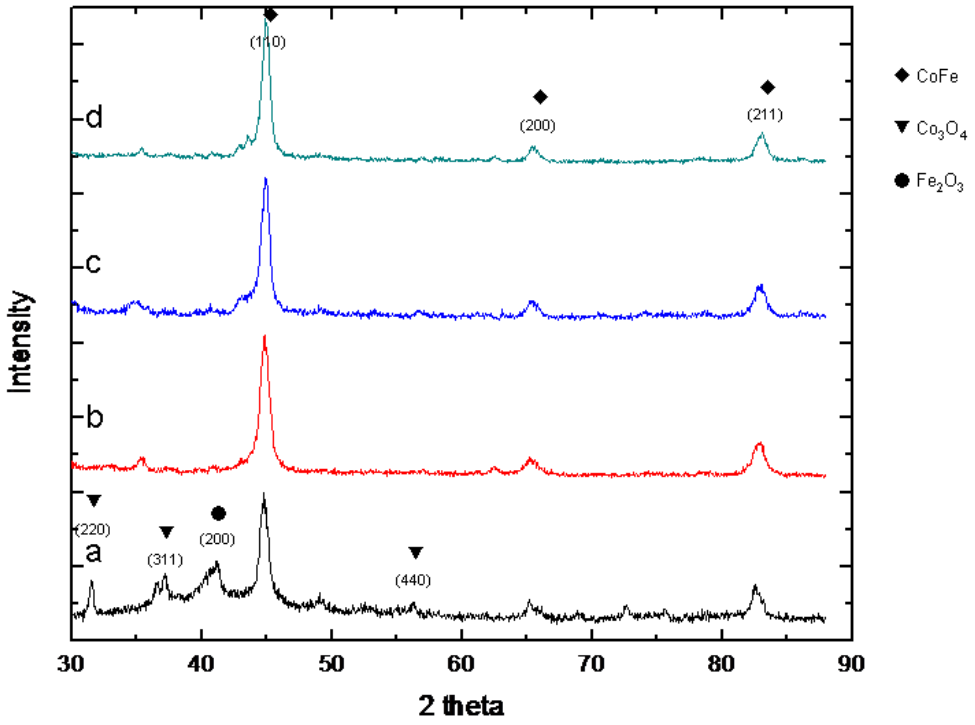


Figure 6.14 XRD patterns of CoFe synthesis with different HDD amount a) 0 mmole b) 2 mmole, c) 5 mmole, and d) 8 mmole.

Without HDD addition although the forming gas has some reducing ability, most of cations can't be reduced into atoms and formed the CoFe nanocrystals. Figure 6.14 a shows the XRD pattern of the mixture of $Co_3O_4$, $Fe_2O_3$ and CoFe. Atoms conjugated together and formed Co and Fe particles, which were oxidized easily. The strong reduction came with high growth rate due to the high concentration of metal atoms in solution, but it also affected the time for nucleation. The proper nucleation and growth rate can be controlled by varying the amount of HDD, and nanowires can be obtained in certain condition. Figure 6.15 showed the curve of relation between

saturation magnetization and HDD amount. With 5 mmole HDD, we can synthesize CoFe nanowire with $M_S$ in 91.25emu/g.

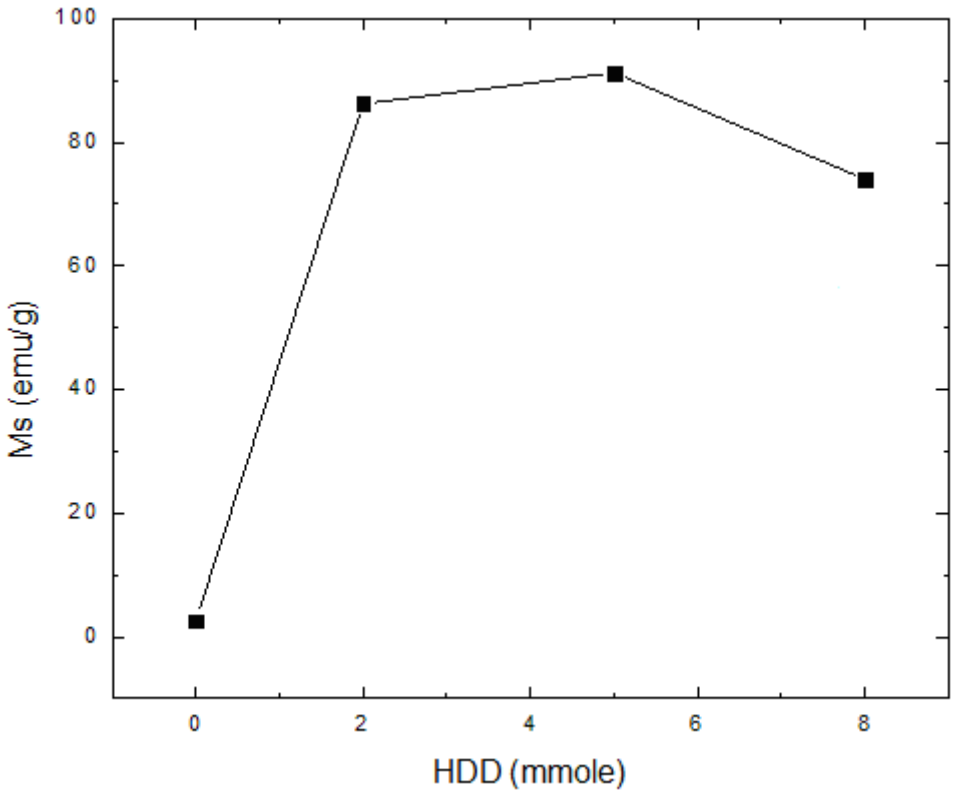


Figure 6.15 The saturation magnetization of CoFe nanocrystals with different HDD amount.

*6.3.4 Effect of Heating Rate*

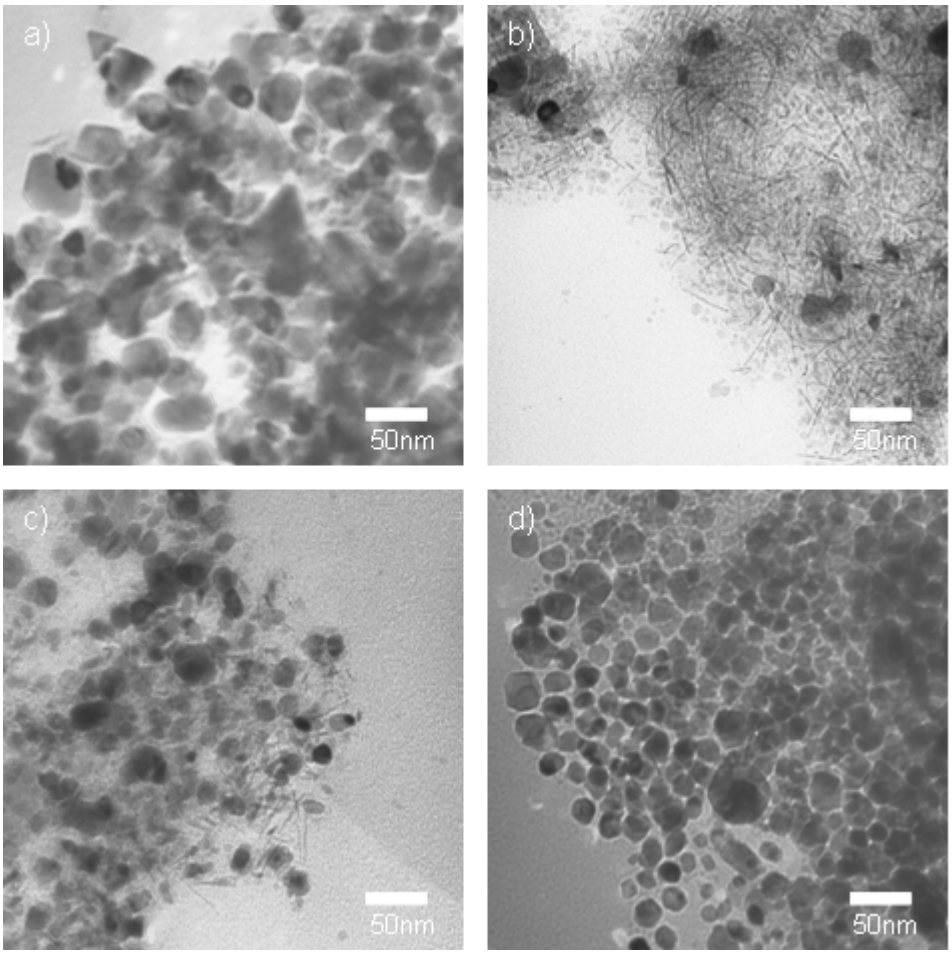


Figure 6.16 TEM images of CoFe nanocrystals synthesized with different heating rate (a) 15℃/min (b) 10℃/min (c) 5℃/min (d) 2℃/min

In these experiments, the heating rate from 200℃ to 300℃ of reaction was very important for nanocrystal growing. With increasing heating rate, there was more energy supplied during the heating process, the nucleation rate and growth rate were also increased. The formation of nanowires was very sensitive to heating rate. It was found that the nanoparticles were formed when the heating rate was 2℃/min(Figure 6.16(d)),

but the mixture of nanoparticles and nanowires were obtained with heating rate increasing to 5℃/min(Figure 6.16(c)), . By increasing heating rate to 10℃/min, most of products are nanowires(Figure 6.16(b)). Nanoparticles was formed again when heating rate was higher than 15℃/min(Figure 6.16(a)). It is observed that the heating rate by controlling the competition between the nucleation and the growth of nanocrystals can be adjusted, with the assistance of surfactants.

## 6.4 Conclusion

CoFe nanowires with 2 nm in diameter and 90 nm in length have been prepared in a reproducible manner by chemical methods. The orientation of nanowires is along (200) direction. The size and shape of nanocrystals can be controlled by adjusting solvent amount and the ratio between surfactants. The best solvent/surfactant condition for CoFe nanowires preparation was found to be 1.2ml OA as solvent and 2.28ml TOP as surfactant. With the different reduction potential, $Fe^{3+}$ and $Co^{2+}$ still can be reduced at the same time by controlling HDD. High yield of CoFe nanowires can be achieved with 5 mmole of HDD. Heating rate is also an important parameter to control the size and shape of nanocrystals. Nanowires can not be formed in the reactions with too high or too slow heating rate, and nanowired can be obtained with proper heating rate at 10 ℃/min. Saturation magnetization ($M_S$) is an important magnetic property of soft materials.

# CHAPTER 7

## SUMMARY AND CONCLUSIONS

In this thesis, synthesis and characterization of ferromagnetic CoNi and CoFe nanocrystals are reported.

The CoNi nanocrystals with different size, shape and composition were successfully synthesized via a chemical solution method. The reduction of nickel and cobalt acetate in a basic solution of 1,2-butanediol leads to formation of CoNi nanocrystals. The growth rate can be controlled by the cobalt/nickel composition and the NaOH concentration. By varying composition in the same synthesis condition, sea-urchin-like shaped particles were obtained with pure cobalt in high growth rate, which favors the growth on the (100) planes in the hcp structure. Isolated CoNi nanowires can be fabricated with a slow growth rate by adding 20% Ni into the composition. By increasing Ni concentration in the composition, the growth rate becomes slower and the growth direction shift to the (002) plane which leads to the formation of the platelet shape. The catalyst amount and surfactants ratio also played an important role on nanowire elongation. The longer nanowires can be prepared by increasing the amount of $RuCl_3$ and the surfactant ratio of TOP/OA. By adjusting the synthesis parameters, the highest $H_C$ of 2.26 KOe was achieved in the $Co_{80}Ni_{20}$ nanowires with 200 nm length and 10 nm diameter CoFe nanocrystals were prepared by non-catalyst chemical solution method. By adjusting the synthesis parameters, such as the ratio of solvent to precursor,

reducing agent amount, heating rate and surfactants ratio, the morphology can be controlled. The growth rate can be controlled by varying reducing agent amount and heating rate. With more reducing agent, more cations were reduced into atoms, leading to a higher growth rate. The higher heating rate also provides more energy for the growth of the nanocrystals. The ratio of solvent to precursor and the ratio of surfactants were the key point in controlling the morphology. With the selective absorption effect, surfactants bonded on (001) planes and cause an anisotropy growth of the (200) plane of the bcc structure. Magnetic properties of these nanocrystals are size and shape dependent. By adjusting the parameters of synthesis condition, the highest $M_S$ of 91.25 emu/g was achieved in CoFe nanowires with 100nm length and 3nm diameter.

In comparison of these two types of magnetic nanowires, the hcp structured CoNi nanocrystals have hard magnetic properties, with high coercivity. Whereas the bcc structured CoFe nanocrystals have soft magnetic properties, with high saturation magnetization. These nanowires with well controlled morphology may find wide applications as building blocks of future advanced magnetic materials.

# APPENDIX A

# UNITS OF MAGNETIC PROPERTIES

## Table A.1 Units of magnetic properties[84]

| Quantity | Symbol | Gaussian & cgs emu [a] | Conversion factor, C [b] | SI & rationalized mks [c] |
|---|---|---|---|---|
| Magnetic flux density, magnetic induction | $B$ | gauss (G) [d] | $10^{-4}$ | tesla (T), $Wb/m^2$ |
| Magnetic flux | $\Phi$ | maxwell (Mx), $G \cdot cm^2$ | $10^{-8}$ | weber (Wb), volt second (V·s) |
| Magnetic potential difference, magnetomotive force | $U$, $F$ | gilbert (Gb) | $10/4\pi$ | ampere (A) |
| Magnetic field strength, magnetizing force | $H$ | oersted (Oe),[e] Gb/cm | $10^3/4\pi$ | A/m [f] |
| (Volume) magnetization [g] | $M$ | $emu/cm^3$ [h] | $10^3$ | A/m |
| (Volume) magnetization | $4\pi M$ | G | $10^3/4\pi$ | A/m |
| Magnetic polarization, intensity of magnetization | $J$, $I$ | $emu/cm^3$ | $4\pi \times 10^{-4}$ | T, $Wb/m^2$ [i] |
| (Mass) magnetization | $\sigma$, $M$ | emu/g | 1<br>$4\pi \times 10^{-7}$ | $A \cdot m^2/kg$<br>Wb·m/kg |
| Magnetic moment | $m$ | emu, erg/G | $10^{-3}$ | $A \cdot m^2$, joule per tesla (J/T) |
| Magnetic dipole moment | $j$ | emu, erg/G | $4\pi \times 10^{-10}$ | Wb·m [i] |
| (Volume) susceptibility | $\chi$, $\kappa$ | dimensionless, $emu/cm^3$ | $4\pi$<br>$(4\pi)^2 \times 10^{-7}$ | dimensionless<br>henry per meter (H/m), Wb/(A·m) |
| (Mass) susceptibility | $\chi_\rho$, $\kappa_\rho$ | $cm^3/g$, emu/g | $4\pi \times 10^{-3}$<br>$(4\pi)^2 \times 10^{-10}$ | $m^3/kg$<br>$H \cdot m^2/kg$ |
| (Molar) susceptibility | $\chi_{mol}$, $\kappa_{mol}$ | $cm^3/mol$, emu/mol | $4\pi \times 10^{-6}$<br>$(4\pi)^2 \times 10^{-13}$ | $m^3/mol$<br>$H \cdot m^2/mol$ |
| Permeability | $\mu$ | dimensionless | $4\pi \times 10^{-7}$ | H/m, Wb/(A·m) |
| Relative permeability [j] | $\mu_r$ | not defined | | dimensionless |
| (Volume) energy density, energy product [k] | $W$ | $erg/cm^3$ | $10^{-1}$ | $J/m^3$ |
| Demagnetization factor | $D$, $N$ | dimensionless | $1/4\pi$ | dimensionless |

*a.* Gaussian units and cgs emu are the same for magnetic properties. The defining relation is $B = H + 4\pi M$.
*b.* Multiply a number in Gaussian units by C to convert it to SI (e.g., $1\ G \times 10^{-4}\ T/G = 10^{-4}$ T).
*c.* SI (*Système International d'Unités*) has been adopted by the National Bureau of Standards. Where two conversion factors are given, the upper one is recognized under, or consistent with, SI and is based on the definition $B = \mu_0(H + M)$, where $\mu_0 = 4\pi \times 10^{-7}$ H/m. The lower one is not recognized under SI and is based on the definition $B = \mu_0 H + J$, where the symbol $I$ is often used in place of $J$.
*d.* 1 gauss $= 10^5$ gamma ($\gamma$).
*e.* Both oersted and gauss are expressed as $cm^{-1/2} \cdot g^{1/2} \cdot s^{-1}$ in terms of base units.
*f.* A/m was often expressed as "ampere-turn per meter" when used for magnetic field strength.
*g.* Magnetic moment per unit volume.
*h.* The designation "emu" is not a unit.
*i.* Recognized under SI, even though based on the definition $B = \mu_0 H + J$. See footnote *c*.
*j.* $\mu_r = \mu/\mu_0 = 1 + \chi$, all in SI. $\mu_r$ is equal to Gaussian $\mu$.
*k.* $B \cdot H$ and $\mu_0 M \cdot H$ have SI units $J/m^3$; $M \cdot H$ and $B \cdot H/4\pi$ have Gaussian units $erg/cm^3$.

# APPENDIX B

# RESEARCH ACCOMPLISHMENTS

Award

- Awarded “An Honorable Mention” in November 2008 by NATEA-Dallas

- Awarded “Outstanding Academic Performance” in November 2009 by NATEA-Dallas Scholarship Award (2009)

- Awarded "Scharff Award Scholarship" on March 22, 2009 by University of Texas at Arlington, Department of Physics for research achievements

REFERENCES


1. S. Chikasumi, Physics of Magnetism, John Wiley and Sons (1964).
2. B. D. Cullity, Introduction to Magnetic Materials, Addison-Wesley Publishing (1972).
3. Nicola A. Spaldn, Magnetic Materials: Fundamentals and Device Applications, Cambridge University Press (2003).
4. William D. Callister, Jr., Material Science and Engineering: An Introduction, John Wiley & Sons (2000).
5. Robert C. O· Handley, Modern Magnetic Materials: Principles and Applications, Wiley & Sons (2000).
6. J.C. Anderson, Magnetism and Magnetic Materials, Chapman and Hall ltd. (1968).
7. R. Skomski and J.M,D. Coey, Physical. Review S, 48, 15812 (1993).
8. http://www.aacg.bham.ac.uk/magnetic_materials.
9. J. M. D. Coey, Solid State Communications, 102, 101 (1997).
10. http://www.irm.umn.edu/hg2m/hg2m_c/hg2m_c.html
11. D.C. Jiles, Acta Meterialia, 15, 5907 (2003).
12. E. F. Kneller and R. Hawing, IEEE Transactions on Magnetics, 27, 3588 (1991).
13. J. P. liu, 18th International workshop on high performance magnets and their : applications, Annecy (France) (2004).

14. J. P. liu, Nanosturctured Soft and Hard Magnetic Materials, Kluwer Academic/Plenum Publishers and Tsinghua University Press (2003).

15. J. Sort, S. Surmach, J. S. Munoz, and M. D. Baro, Physical Review B, 65, 174420 . (2002).

16. R. Coehoorn, D. B. de Mooij and C. de Waard, Journal of Ma!Ehm and Magnetic Material, Volume 80, 10 (1989).

17. R. Skomski and J.M.D. Coey, Physical Review B, 48,15812(1993).

18. E. E. Fullerton, J. S. Jiang and S. D. Bader, Journal of M~mjlll and Magnetic naterials, 200, 392 (1999).

19. R. Skomski and J.M.D Coey, IEEE Transactions on Magnetics, 30,607 (1994).

20. S. P. Gubin and Y. A. Koksharov, Neorg. Mater., 38,1287 (2002).

21. D. M. Cox, D. J. Tevor, R. L. Whetten, E. A. Rohlfing, A. Kaldor, Phys. Rev. B, 32,7290 (1985).

22. D. Jales, Introduction to Magnetism and Magnetic Materials; CRC Press (1998).

23. M. P. Morales, S. Veinternillas-Verdaguer, M. I. Montero, C. J. Serna, Chern. Mater. 11, 3058 (1999).

24. M. P. Morales, C. J. Serna, F. Bodker, S. Morup, J. Phys.: Condens. Matter 9, 5461(1997).

25. W. A. de Heer, P. Milani and A. Chatelain, Phys. Rev. Lett., 65, 488 (1990).

26. Y. I. Petrov, E. A. Shafranovskii, Y. F. Krupyanskii and S. V. Esin, Ookl. Akad. Nauk, 379, 357 (2001).

27. X. G. Li, A. Chiba, S. Takahashi and K. Ohsaki, J. Magn. Magn. Mater., 173, 101 (1997).

28. F. Fendrych, L. Kraus, O. Chayka, P. Lobotka, I. Vavra, J. Tous, V. Studnicka and Z. rait, Monatsh. Chern., 133,773 (2002).

29. B. Martinez, A. Roig, X. Obradors and E. Molins, J. Appl. Phys., 79, 2580 (1996).

30. V. I. Petrov and E. A. Shafranovskii, Izv, Akad. Nauk, Ser. Fiz., 64,1548 (2000).

31. r A. de Heer, P. Milani and A. Chatelain, Phys. Rev. Lett., 65, 488 (1990).

32. Y. I. Petrov, E. A. Shafranovskii, Y. F. Krupyanskii and S. V. Esin, Dok!. Akad. Nauk, 379, 357 (2001).

33. J. A. Becker, R. Schafer, J. R. Festag, J. H. Wendorff, F. Hensel, J. Pebler, S. A. Quaiser,W. Helbug and M. T. Reetz, Surf. Rev. Lett., 3, 1121 (1996).

34. C. Pascal, J. L. Pascal, F. Favier, M. L. E. Moubtassirn and C. Payen, Chern. Mater., 11,141 (1999).

35. T. Hyeon, S. S. Lee, J. Park, Y. Chung and H. B. Na, J. Am. Chern. Soc., 123, 12798 (2001).

36. A. D. Pomogailo, A. S. Rozenberg and I. E. Uflyand, Metal Nanoparticles in polymers, Khimiya (2000).

37. T. Prozorov, G. Kataby, R. Prozorov and A. Gedanken. Thin Solid Films, 340,189 (1999).

38. C. B. Murray, S. Sun, W. Gaschler, H. Doyle, T. A. Betley and C. R. Kagan, IBM J. 1Res. Dev., 45, 47 (2001).

39. C. B. Murray, S. Sun, H. Doyle and T. A. Betley MRS Bull., 26, 985 (2001).

40. D. R. Uhlmann, G. Teowee and J. Boulton, J. Sol-Gel Sci. Technol., 8,1083 (1997)

41. P. Bose, S. Bid, S. K. Pradhan, M. Pal and D. Chakravorty, J. Alloys Compd., 343, 192 , (2002).

42. Heremans, J., Thrush, C. M., Lin, Y.-M., Cronin, S., Zhang, Z., Dresselhaus, M. S., and Mansfield, .J. F. Bismuth nanowire arrays: synthesis and galvanomagnetic properties. Phys. Rev. B, 61:2921-2930. (2000).

43. Cheng, Y-T., Weiner, A. M., Wong, C. A., Balogh, M. P., and Lukitsch, M. J.. Stress-induced growth of bismuth nanowires. Appl. Phys. Lett., 81:3248-3250. (2002)

44. Huber, C. A., Huber, T. E., Sadoqi, M., Lubin, J. A., Manalis, S., and Prater, C. B. Nanowire array composites. Science, 263:800-802. (1994).

45. Lin, Y-M., Cronin, S. B., Ying, J. Y, Dresselhaus, M. S., and Heremans, J. P. Transport properties of Bi nanowire arrays. Appl. Phys. Lett., 76:3944-3946. (2000)

46. Zhang, Z., Ying, J. Y, and Dresselhaus, M. S. Bismuth quantum-wire arrays fabricated by a vacuum melting and pressure injection process. J. Mater. Res., 13:1745-1748. (1998)

47. Diggle, J. W., Downie, T. C., and Goulding, C. W. Anodic oxide films on aluminum. Chem. Rev., 69:365-405. (1969)

48. Li, A. P., Muller, F., Birner, A., Neilsch, K., and Gosele, U. Hexagonal pore arrays with a 50-420nm interpore distance formed by self-organization in anodic alumina. J. Appl. Phys., 84:6023-6026. (1998)

49. O'Sullivan, J. P. and Wood, G. C. The morphology and mechanism of formation of porous anodic films on aluminum. Proc. R. Soc. London A, 317:511-543. (1970).

50. Sullivan, J. P. and Wood, G. C. The morphology and mechanism of formation of porous anodic films on aluminum. Proc. Roy Soc. Lond. A., 317:511-543. (1970)

51. Mlawiawi, D. A., Coombs, N., and Moskovits, M. Magnetic-properties of Fe deposited into anodic aluminum-oxide pores as a function of particle-size. J. Appl. Phys., 70:4421- 1425. (1991).

52. Zhang, Z., Gekhtman, D., Dresselhaus, M. S., and Ying, J. Y. Processing and characterization of single-crystalline ultrafine bismuth nanowires. Chem. Mater., 11:1659-l665. (1999)

53. Ferre, R., Ounadjela, K., George, J. M., Piraux, L., and Dubois, S. Magnetization processes in nickel and cobalt electrodeposited nanowires. Phys. Rev. B, 56:14066-14075. (1997).

54. Zeng, H., Zheng, M., Skomski, R., Sellmyer, D. J., Liu, Y, Menon, L., and Bandyopadhyay, S. Magnetic properties of self-assembled Co nanowires of varying length and diameter. J. Appl. Phys, 87:4718-4720. (2000)

55. Sun, L., Searson, P., and Chien, C. L. Electrochemical deposition of nickel nanowirearrays in single-crystal mica films. Appl. Phys. Lett., 74:2803-2805. (1999)

56. Mawiawi, D. A., Coombs, N., and Moskovits, M. Magnetic-properties of Fe deposited into anodic aluminum-oxide pores as a function of particle-size. J. Appl. Phys., 70:4421-4425. (1991)

57. Piraux, L., George, I. M., Despres, J. F., Leroy, C., Ferain, E., Legras, R., Ounadjela, K., and Fert, A. Giant magnetoresistance in magnetic multilayered nanowires. Appl. Phys. Lett., 65:2484-2486. (1994)

58. Blondel, A., Meier, J. P., Doudin, B., and Ansermet, J.-P. Giant magnetoresistance of nanowires of multilayers. Appl. Phys. Lett., 65:3019-3021. (1994)

59. Bhattacharrya, S. and Saha, S. K. Nanowire formation in a polymeric film. Appl. Phys. Lett., 76:3896-3898. (2000)

60. Routkevitch, D., Bigioni, T., Moskovits, M., and Xu, J. M. Electrochemical fabication of CdS nanowire arrays in porous anodic aluminum oxide templates. J. Phys. Chem., 100: 14073-14047. (1996)

61. Almawlawi, D., Liu, C. Z., and Moskovits, M. Nanowires formed in anodic oxide nanotemplates. J. of Mater. Res., 9:1014-1018. (1994)

62. Cheng, G. S., Zhang, L. D., Chen, S. H., Li, Y, Li, 1., Zhu, X. G., Zhu, Y, Fei, G. T., and Mao, Y. Q. Ordered nanostructure of single-crystalline GaN nanowires in a honeycomb structure of anodic alumina. J. Mater. Res., 15:347-350. (2000)

63. Berry, A. D., Tonucci, R. J., and Fatemi, M. Fabrication of GaAs and InAs wires in nanochannel glass. Appl. Phys. Lett., 69:2846-2848. (1996)

64. Zhanqiang Deng., Junjie Qi., Yue Zhang., Qingliang Liao., Yunhua Huang and Jiawei Cao. Synthesis, Structure and Growth Mechanism of ZnS Nanowires with High Aspect Ratio. Acta Physico-Chimica Sinica.,(2008)

65. Gates, B., Yin, Y, and Xia, Y. A solution-phase approach to the synthesis of uniform nanowires of crystalline selenium with lateral dimensions in the range of 10-30 nrn. J. A.m. Chem. Soc., 122:12582-12583. (2000)

66. Gates, B., Mayers, B., Cattle, B., and Xia, Y. Synthesis and characterization of uniform nanowires of trigonal selenium. Adv. Funct. Mat., 12:219-227. (2002)

67. Mayers, B., Gates, B., Yin, Y., and Xia, Y. Large-scale synthesis of mono disperse nanorods of se/te alloys through a homogeneous nucleation and solution growth process. . Adv. Mat., 13:1380-1384. (2001).

68. Peng, X., Wickhmn, .J., and Alivisatos, A. P. Kinetics of II-VI and III-V colloidal ,semiconductor nanocrystal growth: 'Focusing' of size distributions. J. Am. Chem. Soc., 120:5343-5344. (1998)

69. Manna, L., Scher, E. C., and Alivisatos, A. P. Synthesis of soluble and processable rod-, arrow-, teardrop-, and tetrapod-shaped CdSe nanocrystals. J. Am. Chern. Soc., 122: 12700-12706. (2000)

70. Bashouti, M., Berger, S., and Lifshitz, E. Synthesis and characterization of PbSe quantum-wires, multi-pods, and cubes. in press. (2002)

71. V. K. La Mer, R. H. Dinegar, J. Am, Chem. Soc., 72, 4847 (1950)

72. V. K. La Mer, Ind. Eng. Chem., 44, 1270 (1952)

73. I. M. Lifshitz, V. V. Slyozov, J. Phys. Chem. Solids, 19,35 (1961)

74. C. Wagner, Z. Elektrochem., 65, 581 (1961)

75. T. Sugimoto, Adv. Collid Interface Sci., 28, 165 (1987)

76. N. Wang et Al. Growth of nanowires, Materials Science and Engineering R 60: 1-51 (2008).

77. J.D Holme, K.P. Johnston, R.C. Doty, B.A. Korgel, Science 287, 1471.(2000)

78. T. Hanrath, BA. Korgel, J. Am. Chem. Soc. 124, 1424 (2002)

79. R.L Penn, J.F. Banfield, Geochim. Cosmochim. Acta 63, 1549 (1999)

80. D.H. Qin, C.W.Wang, Q.Y. Sun, H.L. Li, The effects of annealing on the structure and magnetic properties of CoNi patterned nanowire arrays, Appl. Phys. A 74, 761–765 (2002)

81. D. Ung, Y. Soumare, N. Chakroune, G. Viau, M.-J. Vaulay, V. Richard, F. Fie´vet, Growth of Magnetic Nanowires and Nanodumbbells in Liquid Polyol, Chem. Mater. 19, 2084-2094 (2007)

82. Luo Zhixun, Fang Yan, Zhou Xiaofang, Yao Jiannian. Synthesis of highly ordered Iron/Cobalt nanowire arrays in AAO templates and their structural properties, Materials Chemistry and Physics.

83. A. L. Elı´as, J. A. Rodrı´guez-Manzo, M. R. McCartney, D. Golberg, A. Zamudio, S. E. Baltazar, F. Lo´ pez-Urı´as, E. Mun˜ oz-Sandoval, L. Gu, C. C. Tang, D. J. Smith, Y. Bando, H. Terrones, and M. Terrones. Production and Characterization ofSingle-Crystal CoFe Nanowires Inside Carbon Nanotubes, Nano letter, 2005

84. R. B. Goldfarb and F. R. Fickett, U.S. Department of Commerce, National Bureau of Standards, Boulder, Colorado 80303, March 1985 NBS Special Publication 696

for sale by the Superintendent of Documents, U. S. Government Printing Office, Washington, DC 20402.

# BIOGRAPHICAL INFORMATION

PoChing Tsai was born in Kaohsiung, Taiwan. After graduating from high school, the author received higher education in the Department of Chemistry of Sun Yet-Sen University (Zhongshan University) and earned his Bachelor's Degree of Science in Chemistry there. After the graduation from college, the author felt the need to have a better understating of various materials, which motivated him to continue his graduate education in Material Science. He was admitted into the Department of Material Science and Engineering in the University of Texas at Arlington (UTA), Texas, USA, in 2008. In the author's master program, he worked in the project of synthesis and characterization of magnetic nanowires under the supervising of Dr. J. Ping Liu. Through the work in this project, he has enriched his knowledge and experience in the area of Nano-Magnetism and Nanotechnology, which has drawn a great attention from all over the world. Mr. Tsai is exploring more in the area of Materials Physics, as he will continue to pursue his Doctoral Degree in Material Science and Engineering.